CDF/ANAL/EXOTIC/CDFR/8535
Draft 2.0
October 24, 2006

Search for Technicolor Particle in Association with $W^{\pm}$ Boson at CDF with $\int \mathcal{L}dt$ = 955 pb^{-1}

Tatsuya Masubuchi[1], Yoshio Ishizawa[1], Shinhong Kim[1], Kuni Kondo[2], Yoshiaki Kusakabe[2], Michael. McFarlane[3], Jason Nielsen[3], Anyes Taffard[4], Weiming Yao[3]

[1]*University of Tsukuba*
[2]*Waseda University*
[3]*LBNL*
[4]*University of Illinois Urbana-Champaign*

Abstract

We present a search for Technicolor particles decaying into $b\bar{b}$ and produced in association with $W^{\pm}$ bosons in $p\bar{p}$ collisions at $\sqrt{s} = 1.96$ TeV. The search uses approximately 954.7 pb^{-1} for CEM and CMUP and 941.3 pb^{-1} for CMX of the dataset accumulated by the CDF collaboration at Fermilab Tevatron. Events with an electron or muon, missing E_T and two jets, one of them b-tagged, are selected. The number of tagged events and the invariant mass distributions of $W^{\pm}+2$ jets and dijet are consistent with the Standard Model expectations. We set a 95% confidence level upper limit on the production cross section times branching ratio as a function of the Technicolor particle masses.

1 Introduction

For several decades, the Standard Model has been remarkably successful in explaining and predicting experimental data. However, the mechanism of electroweak symmetry breaking is still not known. The two most popular mechanisms to induce spontaneous symmetry breaking of a gauge theory, resulting in the gauge bosons and fermions acquiring masses, are the Higgs mechanism and the dynamics of a new interaction such as Technicolor. Both mechanisms predict the existence of a new particle X with unknown mass which could be produced at the Tevatron through $p\bar{p} \rightarrow W^{\pm}X$. In this note, we especially present a search for Technirho ($\rho_T^{\pm}$) and Technipion (π_T^0) using the SECVTX b-tagger and LBL NN b-tagger[5, 6]. Technicolor production cross section in pp̄ collisions at $\sqrt{s} = 1.96$ TeV has the order of 1 $\sim$ 5 pb depending on parameter and $m(\rho_T), m(\pi_T)$ mass [1]. Figure 1 shows the Feynman diagrams of Technicolor production searched in this note. In terms of the Higgs boson search, we can refer to [3, 4].

The search signature considered here is $\rho_T^{\pm} \rightarrow W^{\pm}\pi_T^0$ with $W^{\pm} \rightarrow e\nu$ or $\mu\nu$, and $\pi_T^0 \rightarrow b\bar{b}$, giving final states with one high p_T lepton, large missing E_T ($\not\!\!E_T$) and two b jets. We

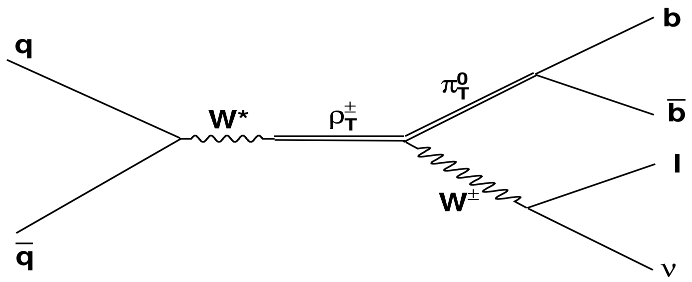

Figure 1: The Feynman diagram of $p\bar{p} \to W^* \to \rho_T^{\pm} \to W^{\pm}\pi_T^0 \to l\nu b\bar{b}$

focus our attention on the $W^{\pm}$ + 2 jets signature since it contains most of the signal, while b-tagged $W^{\pm}+ \geq 3$ jets events are dominated by $t\bar{t}$ decays.

The previous Technicolor search[2] was performed with data corresponding to a integrated luminosity of 161 pb^{-1} and an upper limit on the production cross section was set as observed data is consistent with expected backgrounds.

2 Data sample and Luminosity Calculation

We use the data samples collected up to February 2006. The data up to August 2004 are processed with **Gen5**, and the data after that are processed with **Gen6**. We use the datasets **bhel0d**, **bhel0h** and **bhel0i** (central electron, including ELECTRON_CENTRAL_18 Trigger), and **bhmu0d**, **bhmu0h** and **bhmu0i** (central muon, including MUON_CMUP18, MUON_CMX18 trigger). When we apply the DQM version 13a good run list (bits[1,1,4,1]), the corresponding total integrated luminosity is 954.7 pb^{-1} for CEM and CMUP leptons 941.3 pb^{-1} for CMX muons, and 622 pb^{-1} for CMX keystone and miniskirt.

For the signal acceptance and systematic studies, $\rho_T^{\pm} \to W^{\pm}\pi_T^0$ samples are generated with PYTHIA and the standard Monte Carlo procedure outlined in 5.3.3 for the different $\rho_T^{\pm}$and π_T^0 mass. Figure2 shows the production cross section of $p\bar{p} \to \rho_T^{\pm} \to W^{\pm}\pi_T^0$ as a function of Technipion mass m (π_T^0) for each Technirho mass m ($\rho_T^{\pm}$).

3 Event Selection

Basically we use similar event selection criteria to in the WH search analysis[3, 4] . These events contain an isolated electron or muon with E_T (p_T) $>$ 20 GeV. In this analysis $\not{E}_T$ $>$ 25 GeV is required to reduce NonW background not well-defined for 1 SecVTX tagged event. For double tag events, we keep $\not{E}_T >$ 20 GeV because NonW contamination is already small. Jets are define with $E_T >$ 15 GeV (using a cone of 0.4 and **jetCorr06b** correction level 4) and $|\eta| < 2.0$. To define the tagged sample,we require in addition that one or more jets have a positive thigh-SECVTX tagged jet.

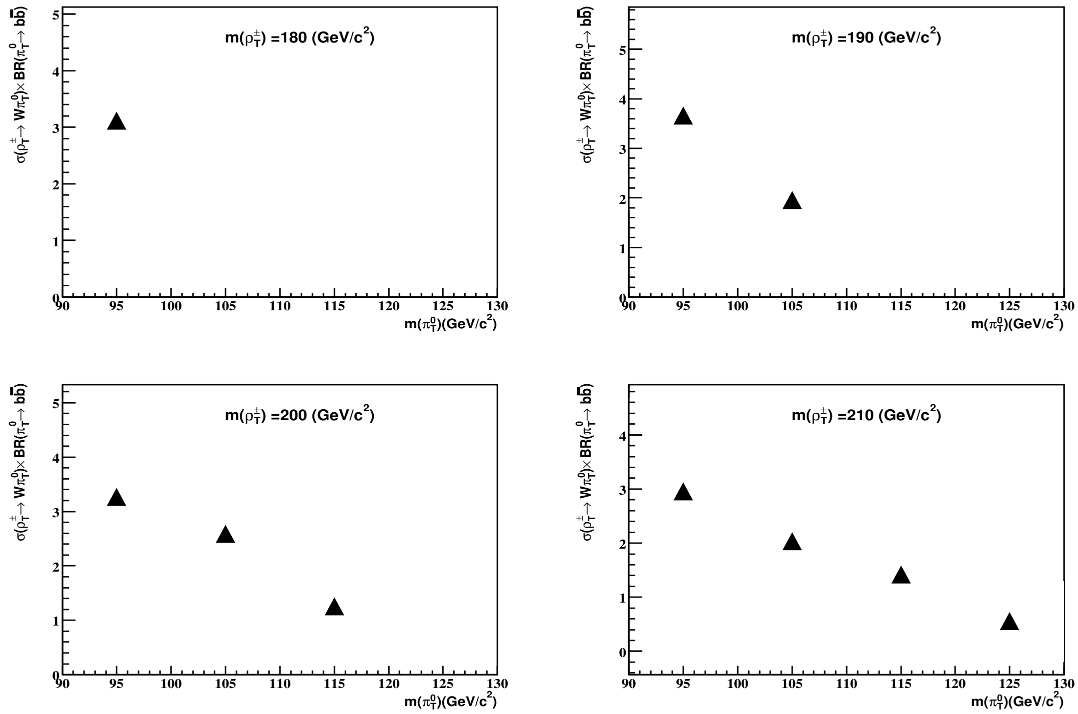

Figure 2: $p\bar{p} \to \rho_T^\pm \to W^\pm \pi_T^0$ production cross section times Branching ratio ($\pi_T^0 \to b\bar{b}$) as a function of the Technipion mass ($m(\pi_T^0\ )$) for different Technirho mass ($m(\rho_T^\pm)$) in pp̄ collisions at $\sqrt{s} = 1.96$ TeV.

4 Neural Network b-tagging

The neural network b-tagger (NNBTAG) builds on the SECVTX secondary vertex tagger to separate the b jets from c and l (light) flavor jets. Jet variables which provide discrimination for b jets are combined into two neural networks. These networks are trained on and applied to events which have been already tagged by the SECVTX algorithm. A detailed description of the neural network training and validation is given in Refs. [5, 6]; neural network b-tagger is used by WH search analysis and $\sim 10\%$ sensitivity is improved. Therefore we also apply NN b-tagging in addition to SECVTX b-tgging because signal signiture is same as WH and background components are identical. Here we summarize the most important features for the Technicolor search.

The tagger employs two neural networks in series. One is trained to separate b jets from light-flavor jets, and the other, b from c. Jets which pass a cut on both neural network output values are accepted by the tagger. These neural networks are trained and applied only to events which are already tagged by the SECVTX algorithm.

The neural networks take as input the same 16 variables. The following 8 variables are properties of the SECVTX tag: number of tracks, transverse decay length, transverse decay length significance, fit χ^2, pseudo-$c\tau$, vertex mass, vertex p_T divided by the sum of the good tracks' p_T, and vertex pass number. The following 8 variables are independent of the SECVTX vertex, but still have some power to discriminate b from c and l jets: number of good tracks, reconstructed mass of pass 1 tracks, reconstructed mass of pass 2 tracks, number of pass 1 tracks, number of pass 2 tracks, total p_T of pass 1 tracks divided by jet p_T, total p_T of pass 2 tracks divided by jet p_T, and jet probability value.

The network output spectra are well-modeled in our simulation. Figure 3 shows the neural network outputs from the $b-l$ network on a sample of SECVTX-tagged heavy-flavor jets from the 8-GeV electron sample and on a sample of tagged light-flavor jets from the jet-20 data.

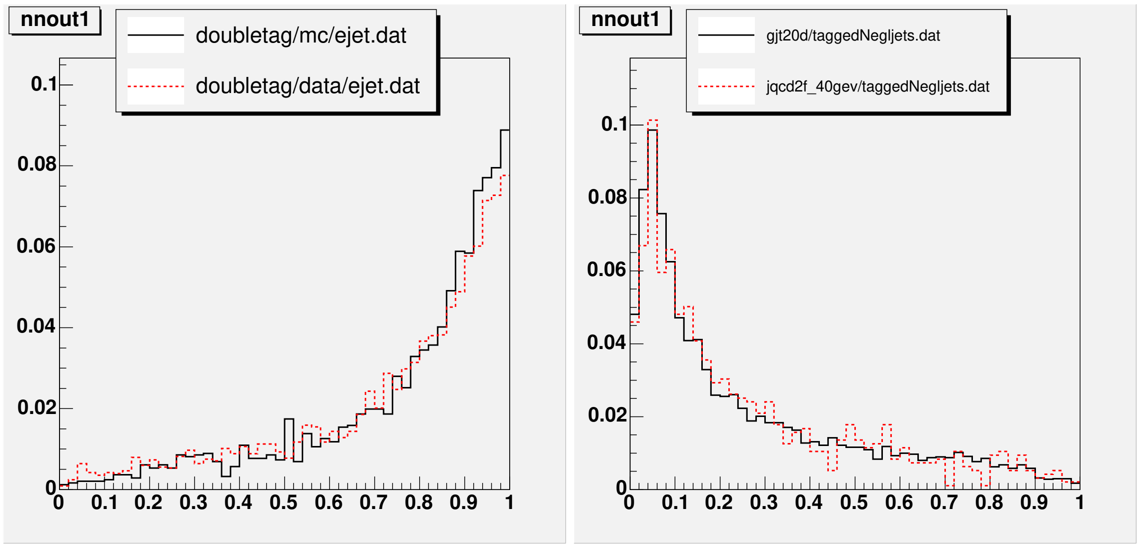

Figure 3: Comparisons of NN b-tag output in data and Monte Carlo for SECVTX-tagged heavy-flavor-enriched jets (left) and tagged light-flavor jets (right).

We choose to set the cut value for 90% b efficiency (after the SECVTX efficiency), corresponding to a value of $NN_{bl} = 0.182$ and $NN_{bc} = 0.242$. The scale factor, measured from the electron sample in the `0h` and `0i` datasets, is 0.97 ± 0.02. (Note that this is the additional scale factor on top of the SECVTX scale factor, applicable because all of the jets under consideration have already been tagged by SECVTX.) We have studied the jet rejection at these cut values, and find that we reject 65% of light-flavor jets and about 50% of the c jets.

We confirm Technicolor signal acceptance is able to keep 90% after applying NN b-tagging for each mass sample.

5 Background Estimation

The background components are based on WH search and $t\bar{t}$ lepton+jets cross section measurement analysis. The following backgrounds sources are considered in the W+jets sample:

- Non-W QCD
- Mistags or false tag due to vertex and track resolution
- W + heavy flavor ($Wb\bar{b}, Wc\bar{c}$) and Wc
- Z + heavy flavor
- Monte Calro-derived background ($t\bar{t}$, single top, diboson (WW,WZ and ZZ) and $Z \rightarrow \tau\tau$)

The background components except for Z + heavy flavor background are estimated in WH search analysis. Basically same background estimate procedures are applied for these background components. But NonW background is re-estimated for one tag w/ NN tag to change $\not\!\!E_T$ selection in signal region. We state Z + jets background estimation in the following section, too.

5.1 NonW(QCD fake) background

To estimate the number of events in which QCD jets fakes a lepton, we use the $\not\!\!E_T$ vs Isolation method. This method is applied in some analysis as Higgs, Top . In previous analysis $\not\!\!E_T$ $>$ 20 GeV was required as signal region. But NonW contamination is still huge around $\not\!\!E_T$ 20 GeV. Some methods[13],[14],[15] is tried to model NonW background but All method is not enough to model NonW background completely. Therefore we apply $\not\!\!E_T > 25$ to reduce dramatically this NonW background for exact one tag with NNtag events. We don't apply $\not\!\!E_T$ $>$25 due to enough small NonW contribution and keep $\not\!\!E_T$ $>$20 for double tag events. We divide the $\not\!\!E_T$ vs isolation plane into the following regions:

- region A: Isolation > 0.2 and $\not\!\!E_T < 15$ GeV
- region B: Isolation < 0.1 and $\not\!\!E_T < 15$ GeV
- region C: Isolation > 0.2 and $\not\!\!E_T > 25$ GeV
- region D: Isolation < 0.1 and $\not\!\!E_T > 25$ GeV (Signal region)

NonW background is re-estimated in this new defined region. The calculated NonW-fraction and estimated NonW events is shown in table1,2.

5.2 Mistag

Mistag matrix, mistag asymmetry 1.37$\pm$0.15 is applied to estimate mistag background components. Additional scale factor 1.05$\pm$0.03 for 0h sample, 1.07$\pm$0.05 for 0i sample is applied. Basically use same procedure except for new scale factor for 0i sample

Sample	1jet	2jet	>= 3jet
bhel0d	0.034 ± 0.0084	0.057 ± 0.015	0.069 ± 0.019
bhmu0d	0.014 ± 0.0036	0.020 ± 0.005	0.026 ± 0.008
bhel0h	0.039 ± 0.0098	0.055 ± 0.014	0.064 ± 0.017
bhmu0h	0.015 ± 0.0037	0.018 ± 0.005	0.020 ± 0.006
bhel0i	0.041 ± 0.0102	0.056 ± 0.014	0.070 ± 0.019
bhmu0i	0.014 ± 0.0035	0.019 ± 0.005	0.023 ± 0.007

Table 1: NonW fraction after the subtraction of $t\bar{t}$ and W+jet contribution

Sample	1jet	2jet	3jet	>=4jet
bhel0d	10.98 ± 1.05	7.25 ± 1.39	2.61 ± 0.58	1.71 ± 0.49
bhmu0d	3.41 ± 0.61	2.53 ± 0.49	1.06 ± 0.25	0.80 ± 0.21
bhel0h	14.49 ± 2.78	7.87 ± 1.49	2.51 ± 0.53	1.28 ± 0.35
bhmu0h	4.91 ± 0.88	1.86 ± 0.35	0.51 ± 0.11	0.73 ± 0.17
bhel0i	$10.24 \pm 0.1.89$	4.51 ± 0.83	1.64 ± 0.34	1.30 ± 0.34
bhmu0i	3.23 ± 0.58	2.14 ± 0.42	0.27 ± 0.064	0.58 ± 0.20

Table 2: Estimated NonW number using new NonW fraction

5.3 W+heavy flavor

Use same procedure as WH analysis, Z+jet contribution is subtracted from W+jets event additionally to avoid double counting

$$N^{HF}_{events} = [N^{pretag}_{events} \times (1 - F_{nonW}) - N_{EWK} - N_{Z+jets}] \times F_{HF} \times \epsilon_{btag}$$

where, F_{HF} is heavy flavor fraction of W+jets events and ϵ_{tag} means tagging efficiency of W+HF. Same value as WH analysis[3] is applied.

5.4 Z+heavy flavor

Some Z+ jets events which fail the standard Z removal contribute to the W+jets sample. We reestimate Z+jets contribution into W+jets events. Z+jets background is calculated in the similar way to W+HF background estimated.

$$N_{Z+HF} = N^{pretag}_{Z+jets} \times f_{ZHF} \times \epsilon_{tag}$$

where N_{Z+jets} is the number of Z+jets before b-tagging, f_{ZHF} is heavy flavor fraction of Z+jets, ϵ_{tag} is tagging efficiency. In [11], it is reported that the fraction of $Zc\bar{c}$ events(including Zc) is a factor of 2.0 larger than the fraction of $Wc\bar{c}$, and the fraction of $Zb\bar{b}$ events is a factor of 2.0 larger than the fraction of $Wb\bar{b}$. In this analysis the value multiplying the above factors with the heavy flavor fraction of W+jets is used as f_{ZHF}. same ϵ_{tag} as W+HF tagging

Njet	1 jet	2 jet	3 jet	>=4 jet
Pretag Events	80361	13246	2111	573
Mistag	124.5± 24.4	47.7± 9.6	14.2± 2.9	3.9± 1.1
$Wb\bar{b}$	269.6± 94.5	132.3± 44.8	26.2± 8.1	4.7± 1.5
$Wc\bar{c}$	54.8± 18.0	39.3± 13.5	7.6± 2.6	1.4± 0.5
Wc	161.6± 40.7	31.4± 8.3	3.0± 0.7	0.4±0.1
Z+jets	15.0 ± 6.1	10.8 ± 4.3	4.0 ± 1.5	0.9±0.4
$t\bar{t}$ (6.7pb)	6.6± 1.1	40.2 ± 6.2	80.7± 12.1	93 ± 13.4
Single top	17.1± 1.7	24.2± 2.1	5.0± 0.4	0.8± 0.1
Diboson/Z$\rightarrow \tau\tau$	8.8± 1.5	14.4± 2.4	3.8± 0.6	0.9± 0.2
nonW QCD	28.4± 5.3	16.8± 3.1	5.8± 1.2	4.4± 1.2
Total Bkg	686.5± 126.0	357.0 ± 63.6	150.4± 19.0	110.5± 14.4
Observed events	712	341	156	129

Table 3: MethodII background estimate in exactly 1 tight SECVTX tag /w NN tagged events

efficiency is applied because the heavy flavor from Z+jet is similar to W+jets. N^{pretag}_{Z+jets} is calculated by

$$N^{pretag}_{Z+jet} = \frac{Acc(Z+jet)}{Acc(W+jet)} \frac{\sigma_{Z+jet}}{\sigma_{W+jet}} N^{pretag}_{W+jet}$$

The cross section obtained from PYTHIA MC is not reliable due to leading order calculation but relative contribution is well-defined. We use only the ratio of acceptance calculated from W/Z + jet PYTHIA and cross section ratio is refereed to [12]. Finally N^{pretag}_{Z+jet} is calculated by normalize N^{pretag}_{W+jet} by above factor.

5.5 Background summary

Table 3,4 and Figure 4 summarize the number of observed events along with the estimated background events for exactly 1tag with NN tag and double tag. The expectations are in reasonably good agreement with the $W^{\pm}$+jets data.

Njet	2 jet	3 jet	>=4 jet
Pretag Events	14604	2362	646
Mistag	3.2$\pm$ 0.5	1.5$\pm$ 0.3	1.1$\pm$ 0.2
W$b\bar{b}$	19.2 $\pm$ 6.5	5.1$\pm$ 1.6	0.8$\pm$ 0.3
W$c\bar{c}$	3.0$\pm$ 1.1	0.4$\pm$ 0.1	0.1$\pm$ 0.03
Wc	0.0$\pm$ 0.0	0.0$\pm$ 0.0	0.0$\pm$0.0
Z+jets	1.9 $\pm$ 0.8	0.8 $\pm$ 0.3	0.2 $\pm$ 0.06
$t\bar{t}$ (6.7pb)	10.5 $\pm$ 2.3	29.8$\pm$ 6.5	46.2 $\pm$ 10.0
Single top	4.7$\pm$ 0.8	1.5$\pm$ 0.3	0.3$\pm$ 0.1
Diboson/Z$\to\tau\tau$	1.2$\pm$ 0.2	0.3$\pm$ 0.05	0.3$\pm$ 0.04
nonW QCD	1.5$\pm$ 0.3	1.0$\pm$ 0.2	0.5$\pm$ 0.1
Total Bkg	45.2 $\pm$ 8.4	40.4$\pm$ 7.0	49.5$\pm$ 10.1
Observed events	39	44	65

Table 4: MethodII background estimate in double tagged events

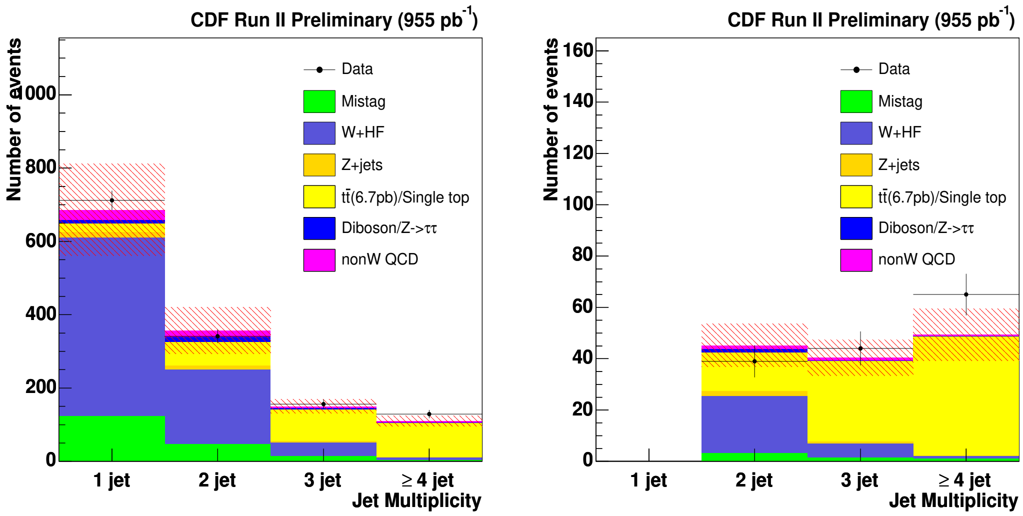

Figure 4: The number of observed positive tagged events and the background summary as a function of jet multiplicity. Left figure means jet multiplicity in 1 SECVTX tag with NN tag and right figure means in double tag.

6 Technicolor Signal Acceptance

To calculate the expected number of signal events $N_{\rho_T^\pm\to\pi_T^0 W\to l\nu b\bar{b}}$, the following equation is used:

$$N_{\rho_T^\pm\to\pi_T^0 W\to l\nu b\bar{b}} = \epsilon_{\rho_T^\pm\to W\pi_T^0\to l\nu b\bar{b}} \cdot \mathcal{L} \cdot \sigma(p\bar{p}\to\rho_T^\pm\to\pi_T^0 W^\pm) \cdot BR(\pi_T^0\to b\bar{b}), \qquad (1)$$

where $\epsilon_{\rho_T^\pm\to W\pi_T^0\to l\nu b\bar{b}}$ is the detection efficiency of signal, $\mathcal{L}$ is the integrated luminosity,

$\sigma(p\bar{p} \to \rho_T^{\pm} \to \pi_T^0 W^{\pm})$ is the Technicolor production cross section in proton anti-proton collisions, and $BR(\pi_T^0 \to b\bar{b})$ is the branching ratio for Higgs boson decay to $b\bar{b}$. The detection efficiency for signal events is defined as:

$$\epsilon_{\rho_T^{\pm} \to W\pi_T^0 \to l\nu b\bar{b}} = \epsilon_{Z0} \cdot \epsilon_{trig} \cdot \epsilon_{leptonid} \cdot \epsilon_{iso} \cdot \epsilon^{MC}_{W\pi_T^0 \to l\nu b\bar{b}} \cdot \left(\sum_{l'=e,\mu,\tau} BR(W \to l'\nu) \right), \qquad (2)$$

where $\epsilon^{MC}_{W\pi_T^0 \to l\nu b\bar{b}}$ is the fraction of signal events (with $|z_0| < 60\,\mathrm{cm}$) which pass the kinematic requirements. The effect of the b-tagging scale factor in this fraction is included by randomly selecting tagged jets to discard. The quantity ϵ_{Z0} is efficiency of the $|z_0| < 60\,\mathrm{cm}$ cut; ϵ_{trig} is the trigger efficiency for high p_T leptons [7, 9]; $\epsilon_{leptonid}$, is the efficiency to identify a lepton; ϵ_{iso} is efficiency of isolation cut [9, 8]; and $BR(W \to l'\nu)$ is the branching ratio for leptonic W decay.

The factor ϵ_{Z0} is measured from data, and ϵ_{trig} is measured from independent backup triggers. The factor $\epsilon_{leptonid}$ involves a "scale factor" that calibrates the MC to the data. We use separate trigger efficiencies, lepton id scale factor and systematic errors for the Gen5 and Gen6 data, where appropriate.

Generated Technicolor samples using PYTHIA MC are 180-210 GeV for $m(\rho_T^{\pm})$ and 95-125 GeV for $m(\pi_T^0)$. These samples are used to estimate Technicolor signal MC efficiency and systematic uncertainty. Figure 5 show the overall acceptance as a function of $m(\pi_T^0)$ for each $m(\rho_T^{\pm})$ in exact 1 SECVTX tag with NN tag and double tag. The signal acceptance obtained from MC is about 0.8% - 1.0% for exact 1 SECVTX tag with NN tag and 0.3%-0.4% for double SECVTX tag. In this figure systematic uncertainties is included in error bar. Signal systematic uncertainty is discussed in the following subsection in detail.

6.1 Systematic Uncertainties on Acceptance

The b-tagging efficiency scale factor in the context of the signal acceptance is included by randomly keeping a fraction of jet tags and discarding the others. The b-tagging efficiency increased by about 4% in the Gen6 run range due to the change in the beam profile. The scale factor S of the b-tagging efficiency is defined as the ratio of single b-jet tagging efficiency in the data to the simulation. It has been measured using the b-enriched inclusive electron and muon samples [10] to be $S = 0.891 \pm 0.071$(stat.+sys.). Although the scale factor for c-tagging efficiency has not been measured, we have no reason to expect it to be very different from the scale factor for b-tagging. We take $S = 0.891 \pm 0.142$ (stat.+sys.) for c-tagging scale factor, with the increased systematic error to account for the additional uncertainty. The scale factor and systematic for NN b-tagging is found to be $S = 0.97 \pm 0.02$.

Other systematic errors in the acceptance include the jet energy scale, initial and final state radiation, lepton identification, and trigger efficiencies. To estimate the systematic uncertainty due to the jet energy scale, we use a mass sample($m(\rho_T^{\pm})$ = 200,$m(\pi_T^0)$ = 115 GeV/c^2) of Technicolor signal. The jet energies in the Technicolor MC samples are shifted by $\pm 1\sigma$, and the difference from the nominal acceptance is taken as the systematic uncertainty.

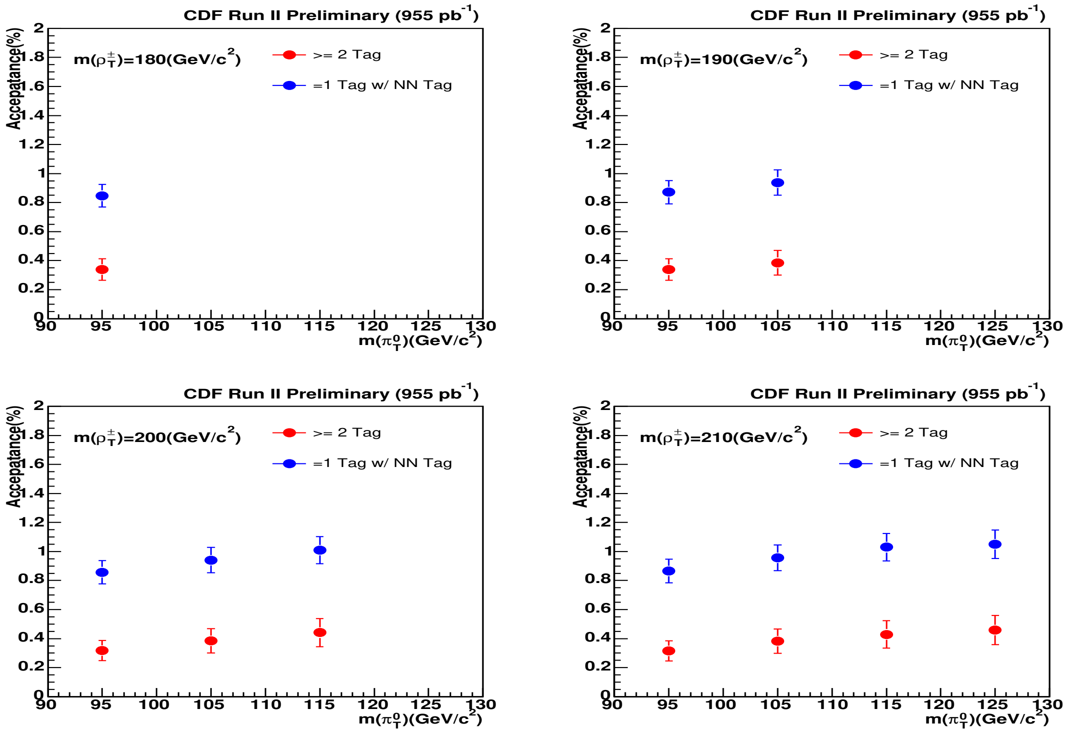

Figure 5: The Technicolor signal acceptance as a function of Technipi mass ($m(\pi_T^0)$) for each Techinirho mass ($m(\rho_T^{\pm})$ in exact one secVtx tag with NN b-tagging. From top left ($m(\rho_T^{\pm}$)=180 GeV, 190 GeV, 200 GeV and 210 GeV

Uncertainties in the lepton identification efficiencies and trigger efficiencies are taken from studies detailed in Refs. [7, 9, 8]. The systematics uncertainties for Gen5 and Gen6 are weighted according to the luminosity. We assign 2% as the lepton ID efficiency systematic uncertainty and less than 1% for the trigger efficiency uncertainty.

The ISR and FSR systematic uncertainties are estimated by changing the parameters related to ISR and FSR from default values to half and double the default values. The difference from the nominal acceptance is taken as the systematic uncertainty.

The parton distribution function uncertainties are evaluated using a re-weighting method. For b-tag scale factor systematic uncertainty, these values we estimate are 5.3% for 1 SECVTX tag with NN tag, 16% for double tag. Each systematic uncertainty and total systematic uncertainties are listed in Table 5 for each b-tagging stage.

6.2 Neutrino solution procedure and reconstructed mass distribution

We perform a direct search for a resonant mass peak in the reconstructed $W^{\pm}+2$ jet and dijet invariant mass distributions with level 7 jet energy correction. To reconstruct the $W^{\pm}+2$ jets mass, we need to determine the p_z of neutrino from $W^{\pm}$ boson. In this analysis we

source	uncertainty(%)	
	=1tag w/ NNtag	double tag
Lepton ID	$\sim 2\%$	$\sim 2\%$
Trigger	$< 1\%$	$< 1\%$
ISR/FSR	6.7%	14%
PDF	1.7%	2.6%
JES	2.8%	3.9%
b-tagging	5.3%	16%
Total	9%	22%

Table 5: Signal systematic uncertainty in each b-tagging stage

apply same procedure of determining the p_z of neutrino as previous analysis [2]. We use $W^{\pm}$ mass constraint in the lepton-neutrino system and take the smaller p_z from the two solutions. If there is no solution for p_z, we take the real part of the solution of the quadratic equation. Figure 6 shows the reconstructed pz of neutrino momentum vs. the generator neutrino momentum using Technicolor signal sample($m(\rho_T^{\pm})$ = 200, $m(\pi_T^0)$ = 115 GeV/c^2) and figure 7 shows reconstructed dijet(Technipi) mass and $W^{\pm}$+2jet mass with reconstructed pz in same signal sample. We use both solution types because it was reported $W^{\pm}$ + 2 jet mass is not different between them in previous analysis.

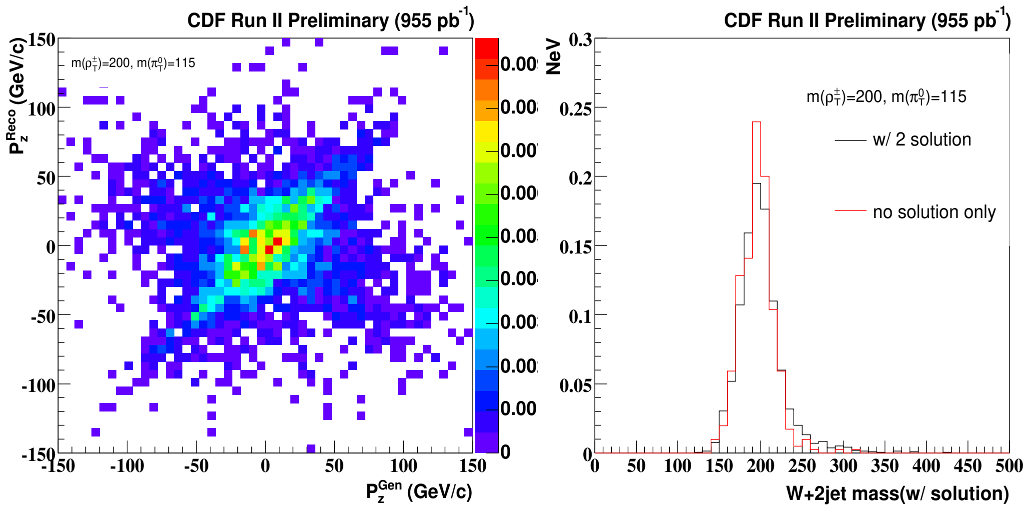

Figure 6: Left: The momentum of z component of reconstructed neutrino vs. the momentum of z component of neutrino in generator level using nominal mass sample ($m(\rho_T^{\pm})$=200 GeV, $m(\pi_T^0)$=115 GeV). Right: The difference of W+2jet mass shapes between w/ 2 solution and no solution case.

Figure 8-9 show reconstructed dijet mass, $W^{\pm}$ + 2jet mass and Q value defined by

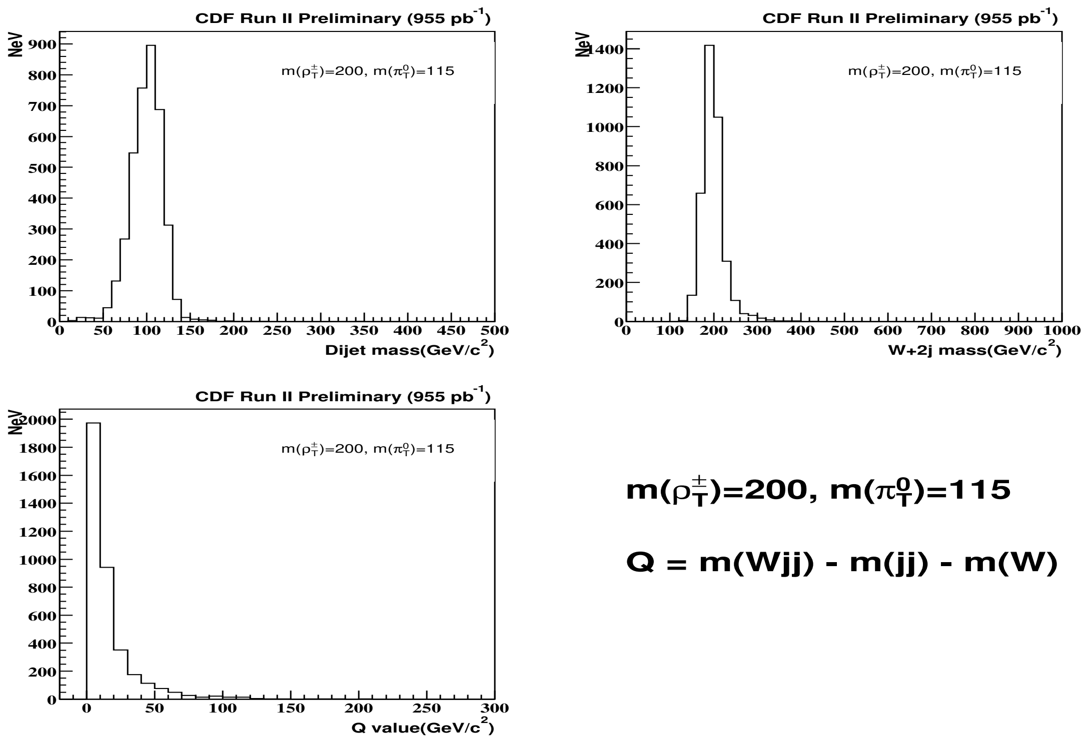

Figure 7: The reconstructed Technipi mass, Technirho mass and Q value in nominal sample ($m(\rho_T^{\pm})$=200 GeV, $m(\pi_T^0)$=115 GeV)

$Q = m(\rho_T^{\pm}) - m(\pi_T^0) - m(W)$ for observed data, expected background and Technicolor signal($m(\rho_T^{\pm})$=200 GeV, $m(\pi_T^0)$=115 GeV) in 1 SECVTX tag with NNtag. Q value and dijet mass are used to calculate 95% C.L. limit. Figure 10-11 show in double tag. According to these plots, observed data shape are consistent with expcted background shape within the uncertainty.

7 Kinematic shape

We check some kinematic distributions for 1tag w/ NNtag and double tag. Figure 12-16 for 1tag w/ NNtag and figure 20-24 show basic lepton, $\not{E}_T$, first leading jet and second leading jet and Transverse mass and Ht. Besides, check other kineamtics in figure 17-19 for 1tag w/ NNtag figure 25-27. Overall distribution is good aggreement between observed data and expected background.

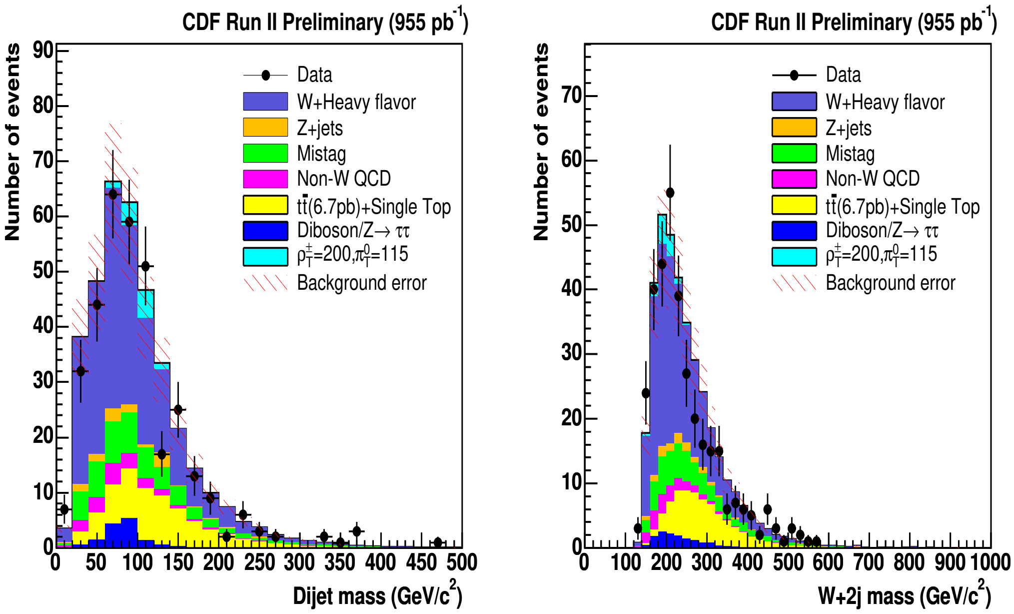

Figure 8: The reconstructed dijet mass and $W^{\pm}$ + 2jet mass distributions of expected background and observed data in exact 1 secVtx tag with NN tag.

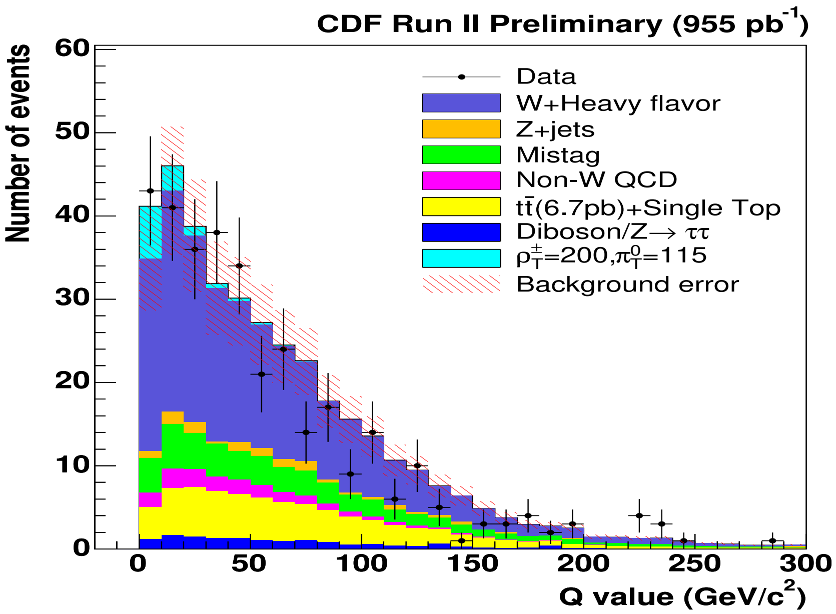

Figure 9: The Q value distribution of expected background and observed data in exact 1 secVtx tag with NN tag

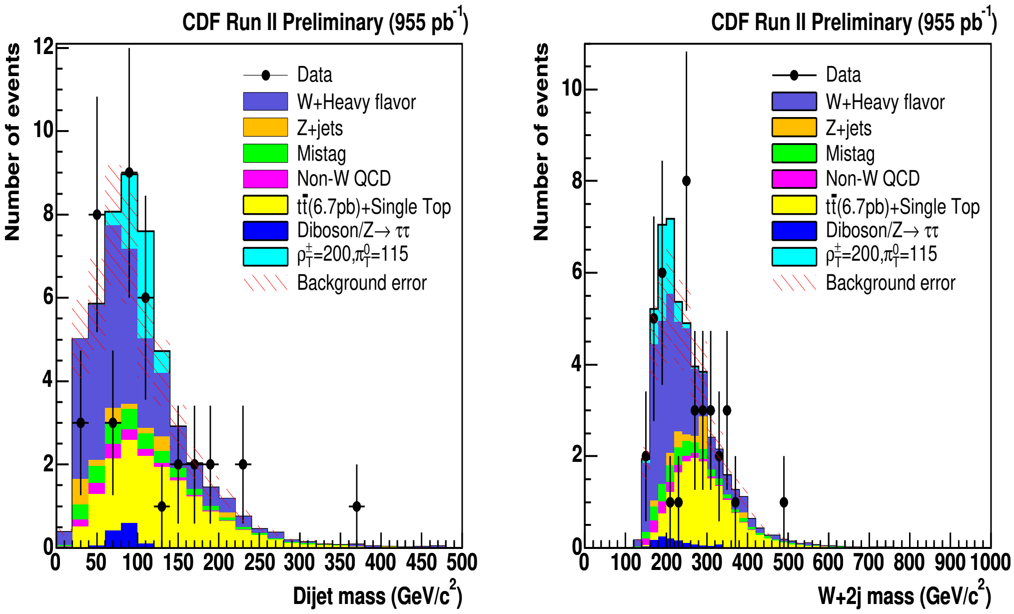

Figure 10: The reconstructed dijet mass and $W^{\pm}$ + 2jet mass distributions of expected background and observed data in double secVtx tag.

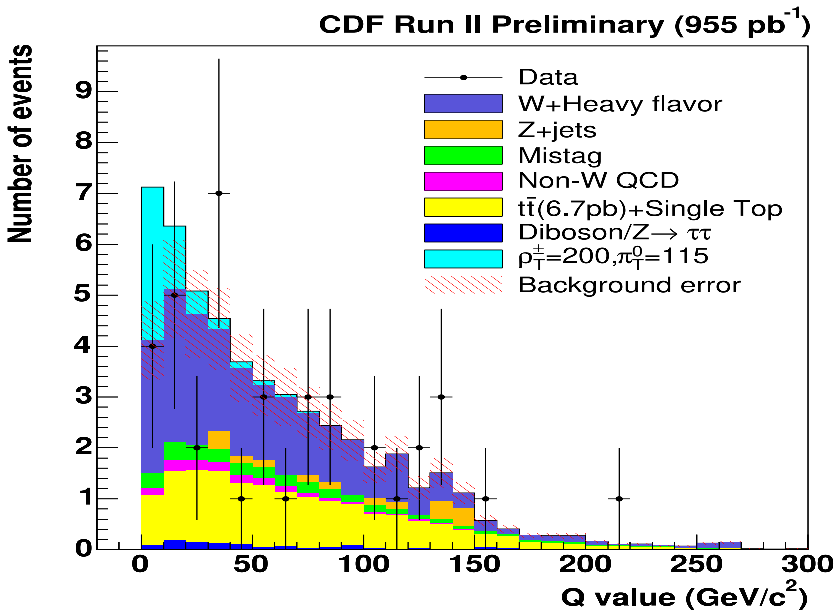

Figure 11: The Q value distribution of expected background and observed data in double tag

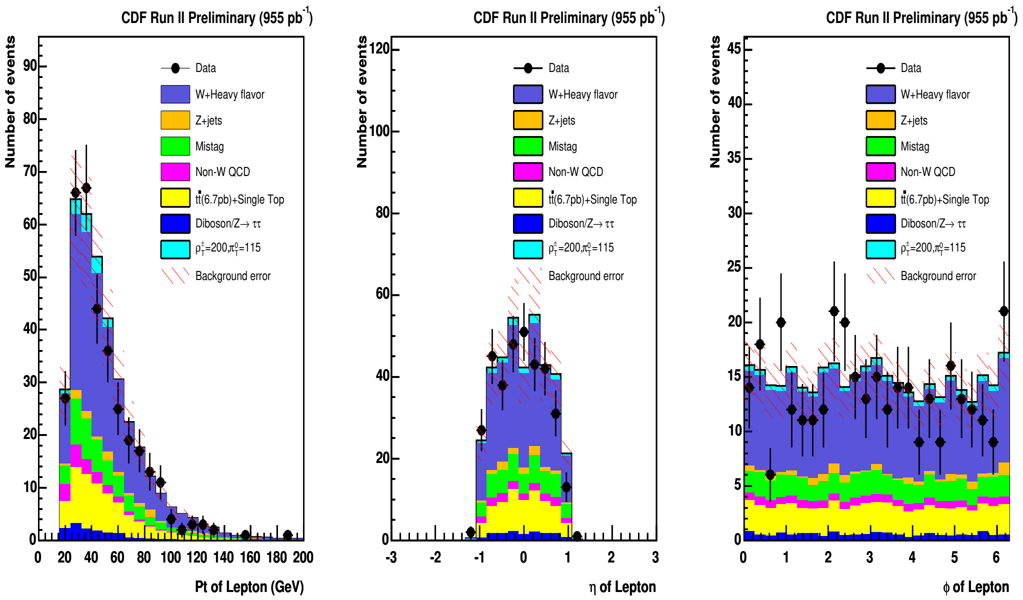

Figure 12: Lepton kinematics using 955pb-1 . From left Lepton p_T , η,ϕ. CEM, CMUP, CMX are included.

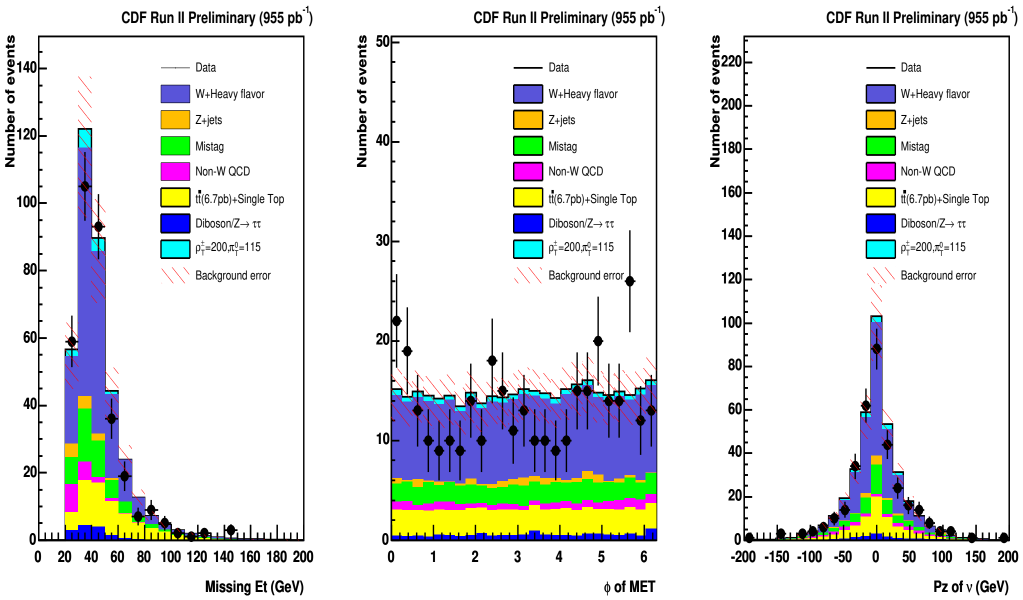

Figure 13: $\not\!\!E_T$ kinematics using 955pb-1 . From left, $\not\!\!E_T$, ϕ of $\not\!\!E_T$ and reconstructed pz of neutrino.

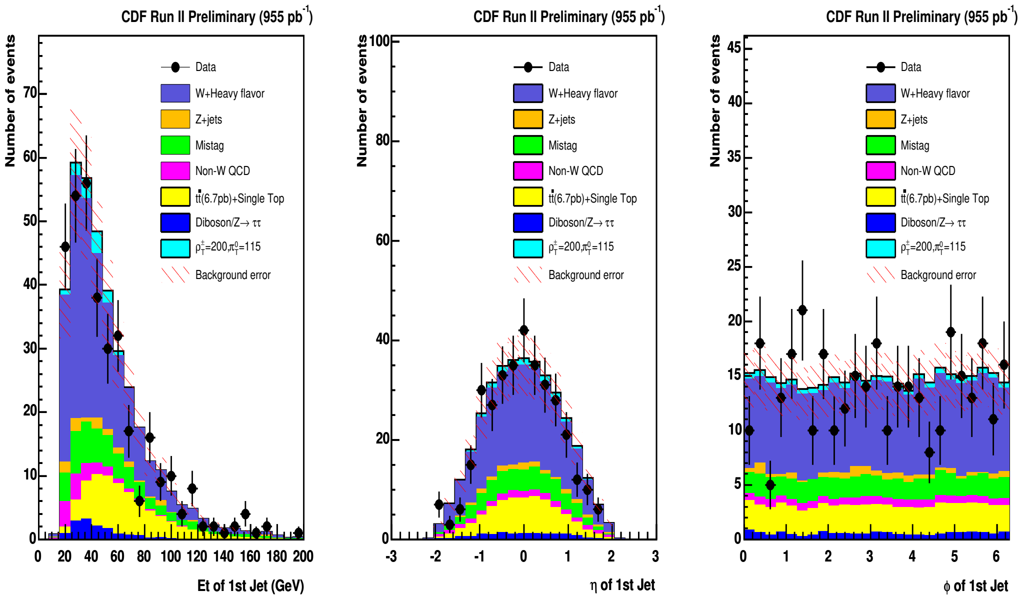

Figure 14: First leading jet kinematics using 955pb^{-1} . From left, E_T of jet, η of jet and ϕ of jet

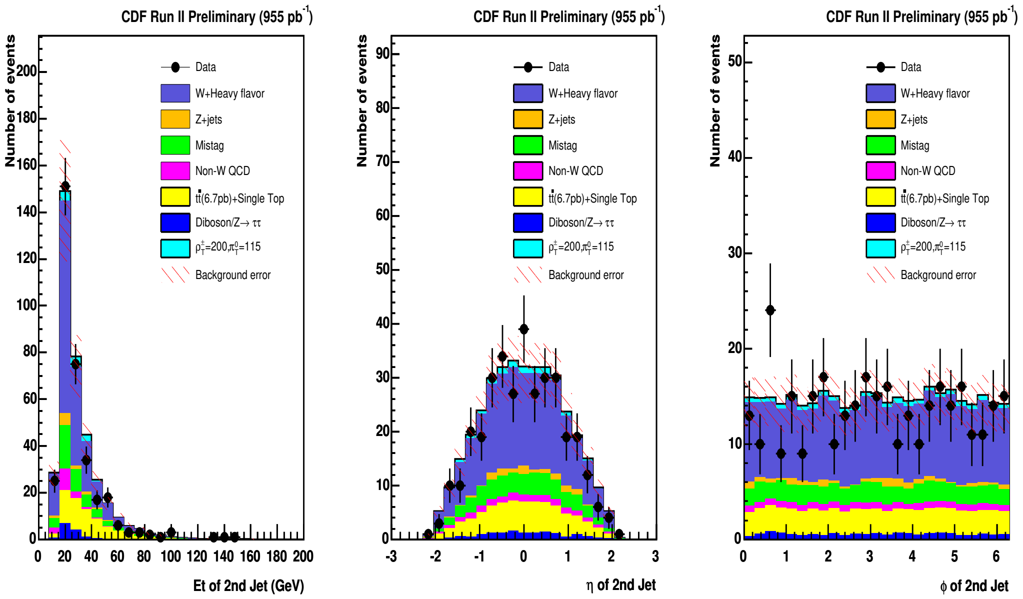

Figure 15: Second leading jet kinematics using 955pb^{-1} . From left, E_T of jet, η of jet and ϕ of jet

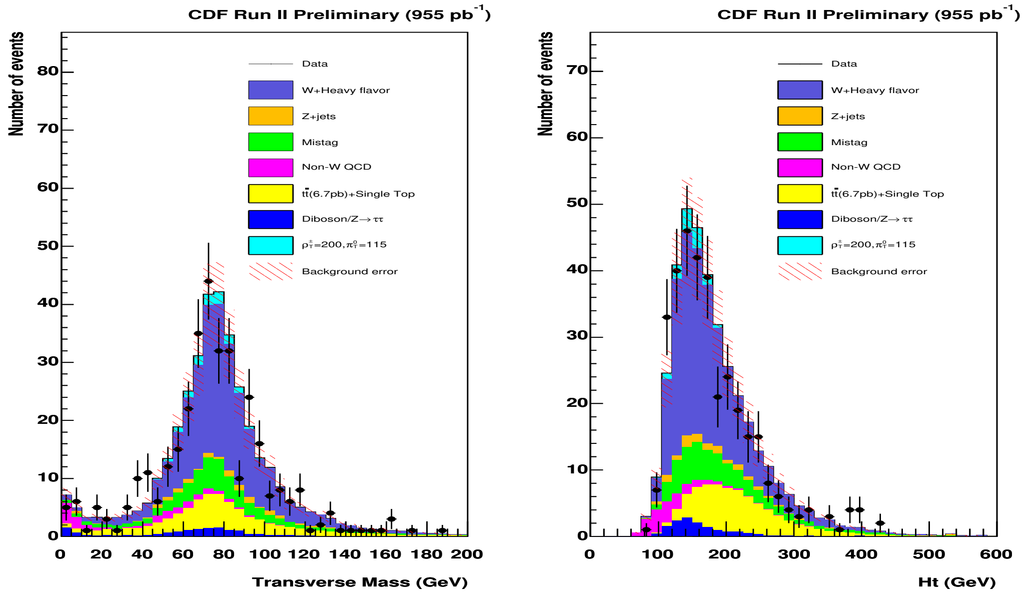

Figure 16: Transverse mass and Ht using 955pb-1

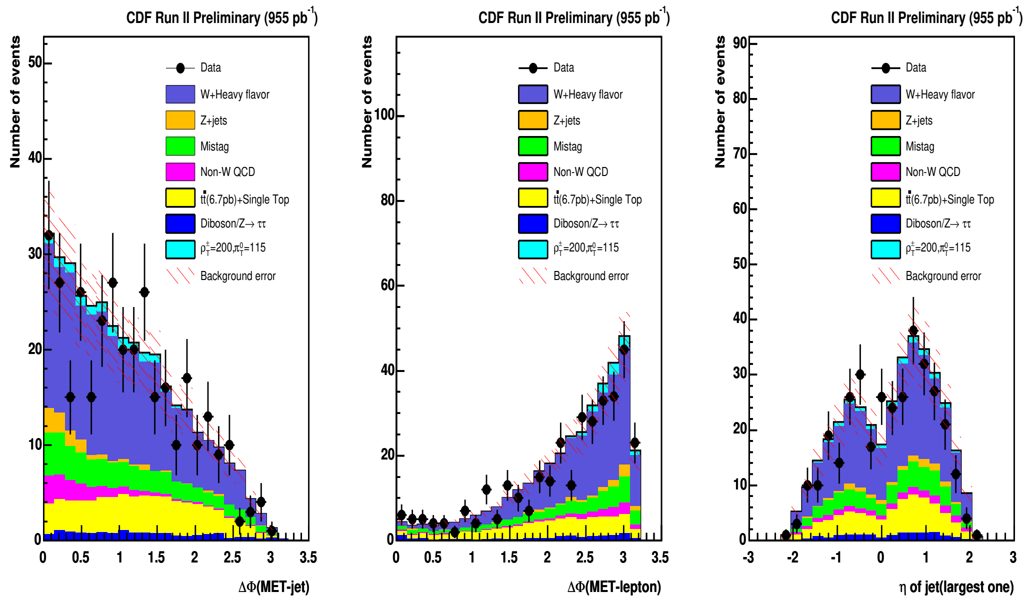

Figure 17: From left, $\Delta\phi$ between $\not\!\!E_T$ and closest jet, $\Delta\phi$ between $\not\!\!E_T$ and lepton and η of jet with largest η using 955pb-1

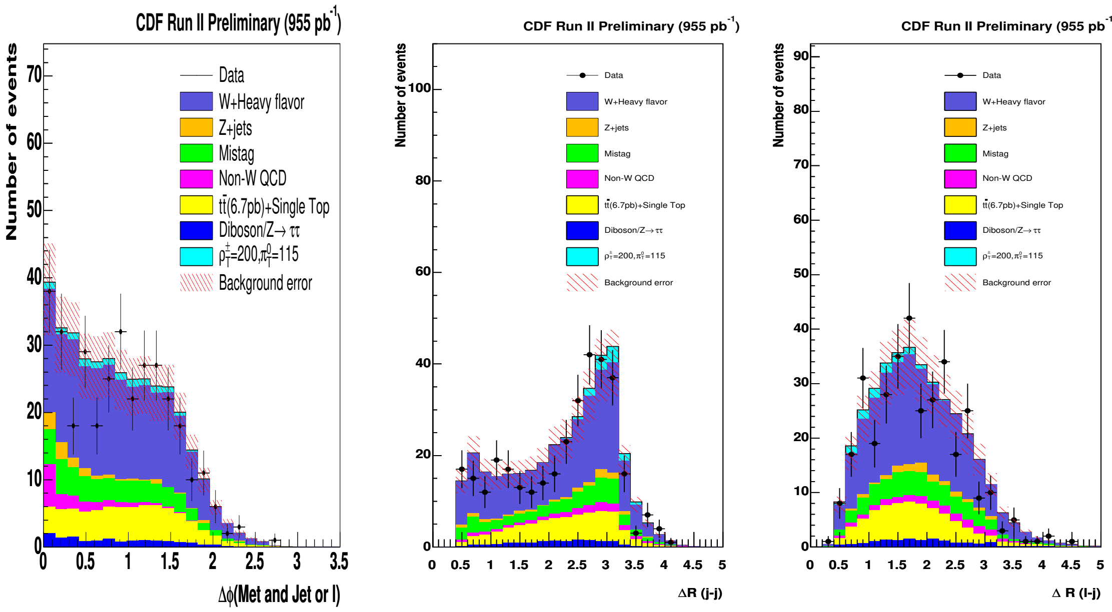

Figure 18: Minimum $\Delta\phi$ between $\not{E}_T$ and lepton or jets, ΔR between 1st jet and 2nd jet, ΔR between lepton and closest jet using 955pb^{-1}

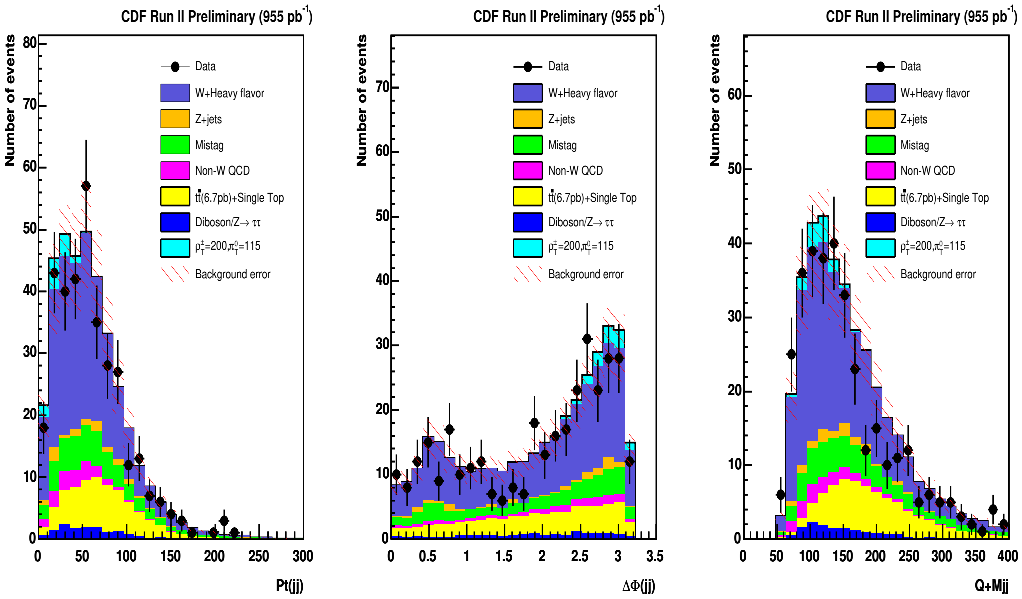

Figure 19: $\Delta\phi$ between 1st jet and second jet, p_T of dijet using 955pb^{-1}

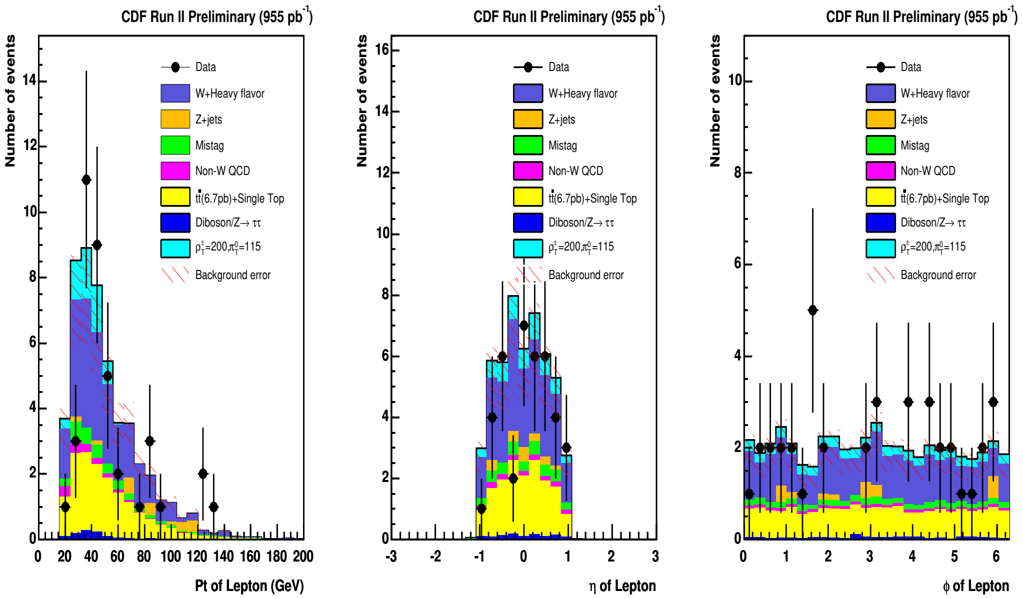

Figure 20: Lepton kinematics using 955pb^{-1} . From left Lepton p_T , η,ϕ. CEM, CMUP, CMX are included.

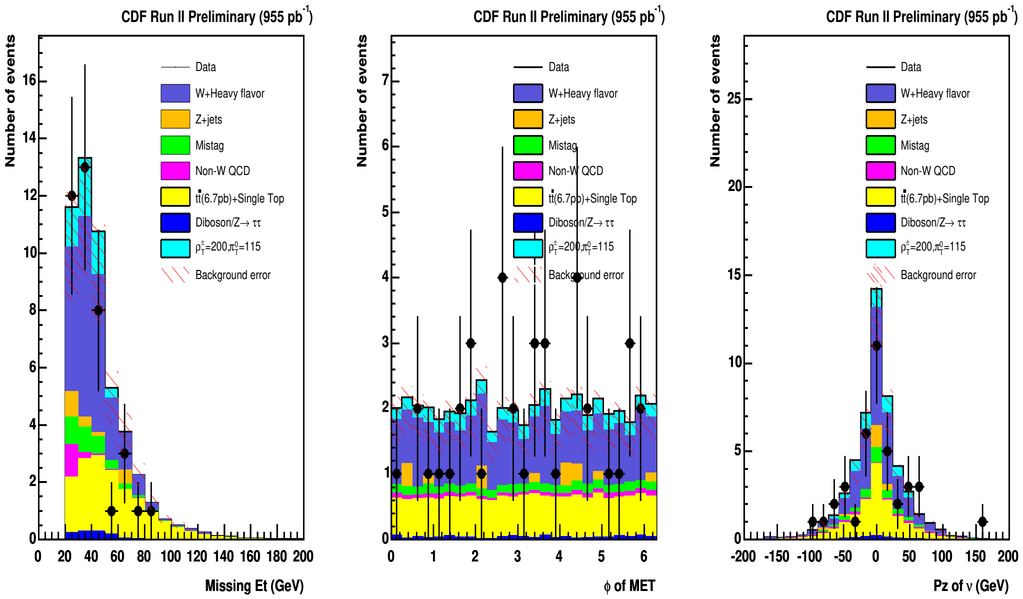

Figure 21: $\not{E}_T$ kinematics using 955pb^{-1} . From left, $\not{E}_T$, ϕ of $\not{E}_T$ and reconstructed pz of neutrino.

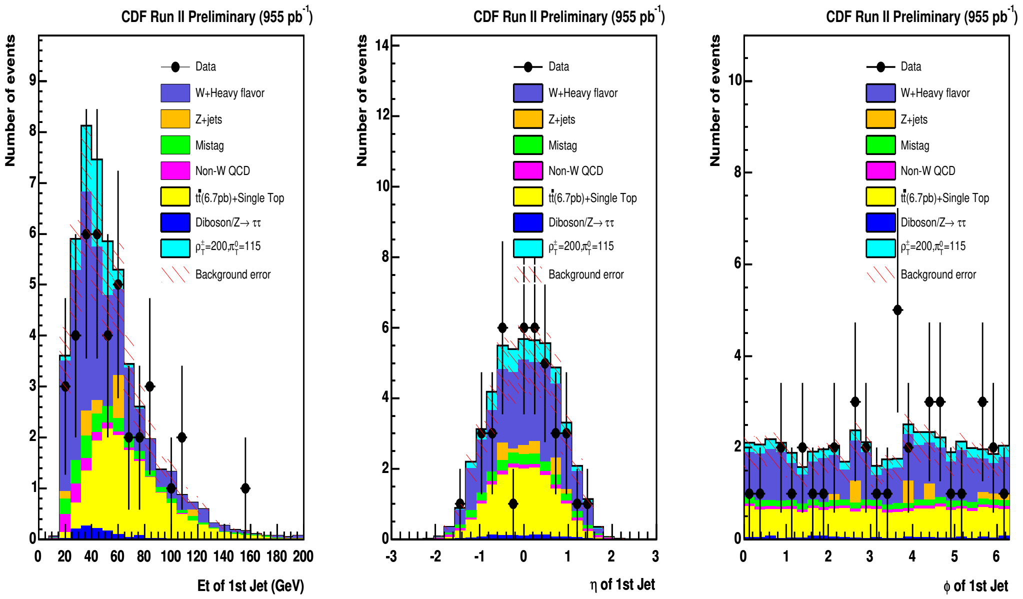

Figure 22: First leading jet kinematics using 955pb^{-1} . From left, E_T of jet, η of jet and ϕ of jet

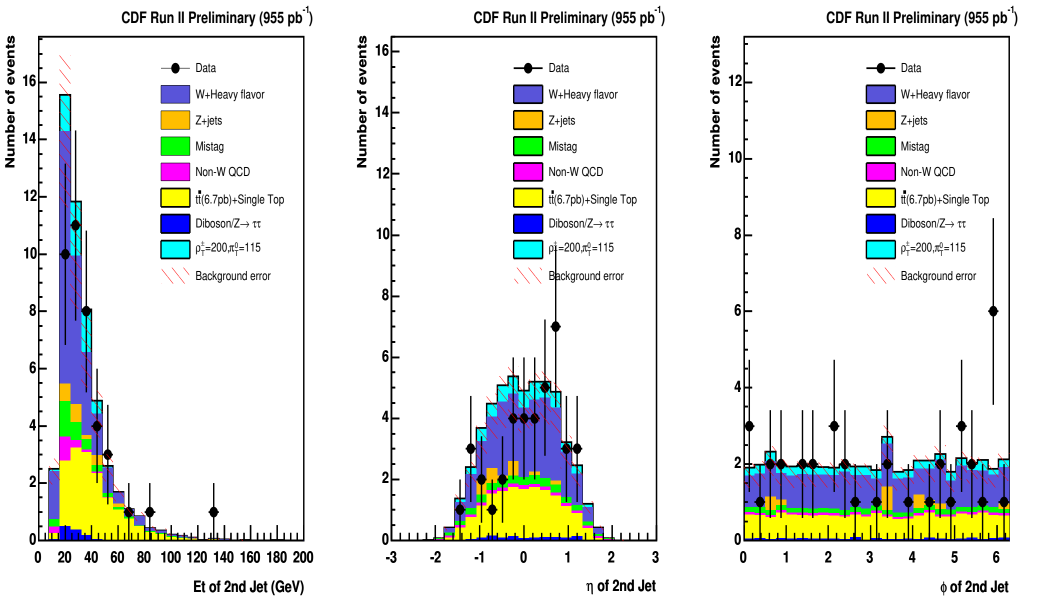

Figure 23: Second leading jet kinematics using 955pb-1 . From left, E_T of jet, η of jet and ϕ of jet

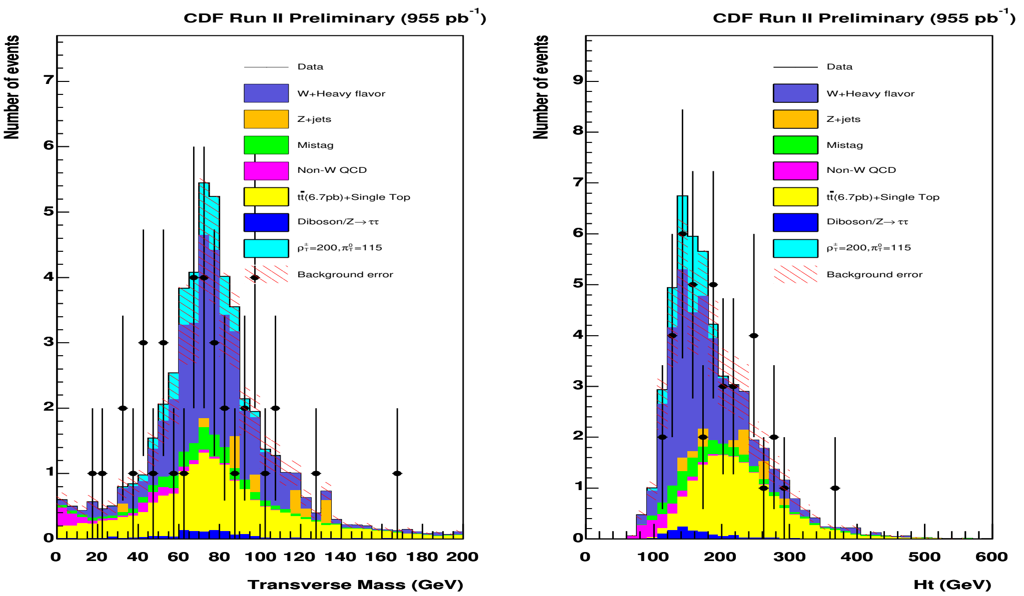

Figure 24: Transverse mass and Ht using 955pb-1

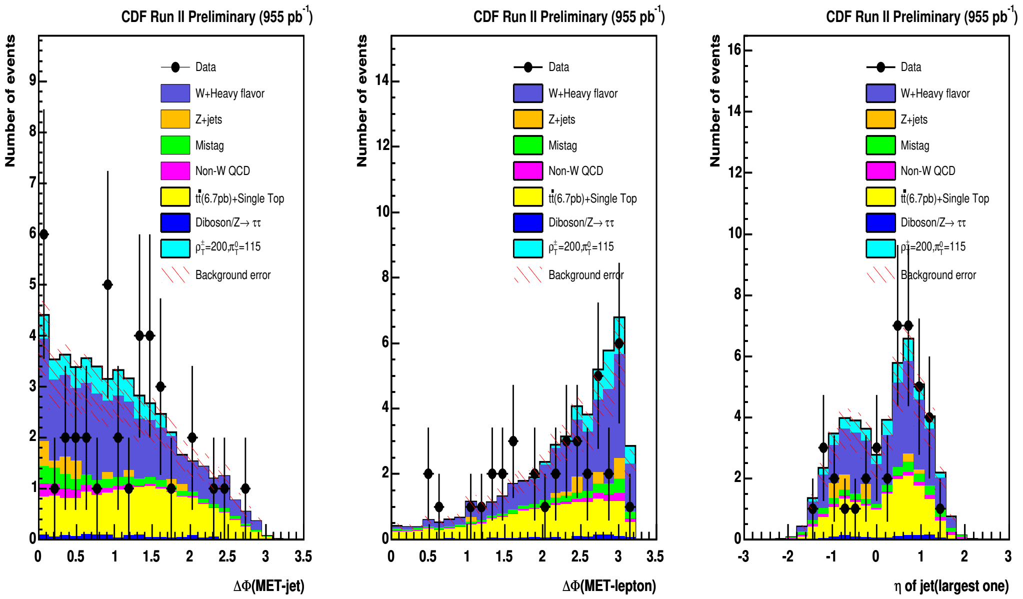

Figure 25: From left, $\Delta\phi$ between $\not{E}_T$ and closest jet, $\Delta\phi$ between $\not{E}_T$ and lepton and η of jet with largest η using 955pb^{-1}

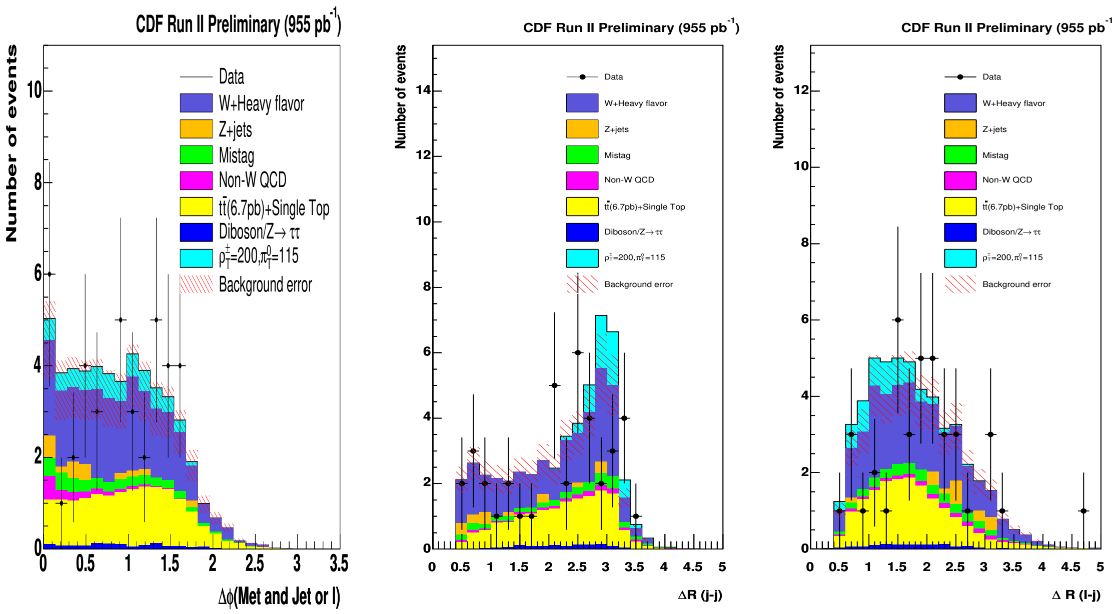

Figure 26: Minimum $\Delta\phi$ between $\not{E}_T$ and lepton or jets, ΔR between 1st jet and 2nd jet, ΔR between lepton and closest jet using 955pb^{-1}

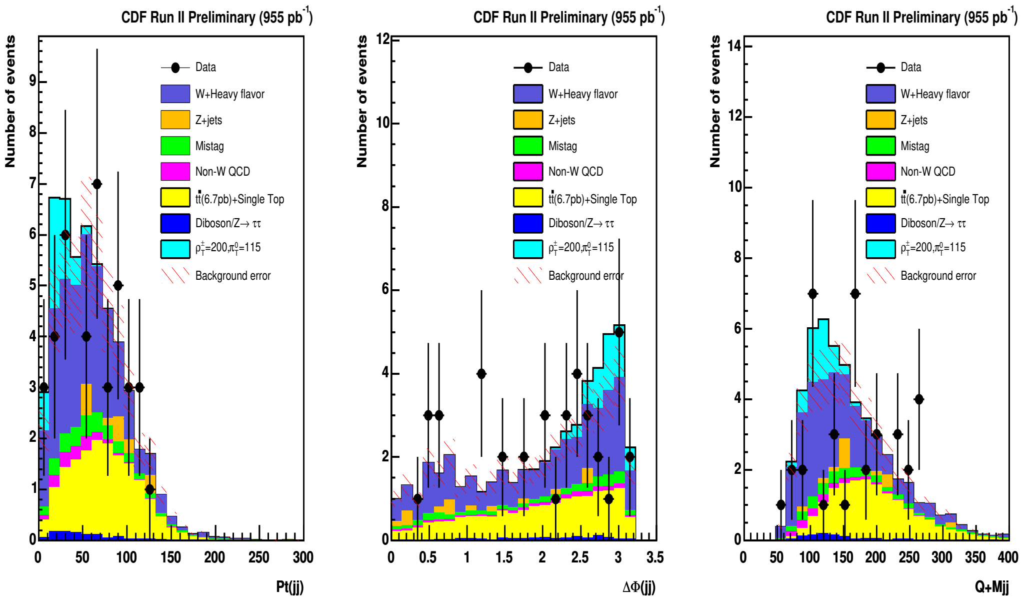

Figure 27: $\Delta\phi$ between 1st jet and second jet, p_T of dijet using 955pb^{-1}

8 95% C.L. upper limit

We set an upper limit on the production cross section times branching ratio of $p\bar{p} \to \rho_T^\pm \to W^\pm \pi_T^0$ as a function of $m(\rho_T^\pm)$ and $m(\pi_T^0)$ by using the number of events in the $W^\pm + 2$ jets sample Since there are no mass peaks observed from $\rho_T^\pm$ and π_T^0,. We assume the $W^\pm + 2$ jets and dijet mass distributions in the data to consist of QCD (mistags, $W^\pm + b\bar{b}$, $W^\pm + c\bar{c}$, $W^\pm + c$ Z+jets and diboson), TOP ($t\bar{t}$ and single top) and $\rho_T^\pm \to W^\pm \pi_T^0$ events. A 2-dimensional binned maximum likelihood technique is used to obtain the limit on the cross section of signal process as in previous analysis. Figure [28-33] show the correlation between the Q value and the dijet mass for $\rho_T^\pm \to W^\pm \pi_T^0 \to \ell\nu b\bar{b}$, $W^\pm + 2$ jets, QCD and TOP. The expected number of events (μ_{ij}) in each mass bin is

$$\mu_{ij} = f_{ij}^{QCD} \cdot N^{QCD} + f_{ij}^{TOP} \cdot N^{TOP} + f_{ij}^{\rho_T^\pm \to W^\pm \pi_T^0} \cdot (\varepsilon \cdot \mathcal{L} \cdot \sigma_{\rho_T^\pm \to W^\pm \pi_T^0}),$$

where f_{ij}^{QCD}, f_{ij}^{TOP} and $f_i^{\rho_T^\pm \to W^\pm \pi_T^0}$ are the expected fraction of events in a given mass bin predicted by Monte Carlo. N^{QCD}, N^{TOP}, ε, $\mathcal{L}$ and $\sigma_{\rho_T^\pm \to W^\pm \pi_T^0}$ are the expected number of QCD and TOP events, the detection efficiency, the luminosity and the unknown $\rho_T^\pm \to W^\pm \pi_T^0$ cross section respectively. In pseudo-experiment, to make the pseudo-data, we fluctuate the number of expected QCD and Top with Gaussian with the estimated total uncertainty independently, and also signal events with total systematic uncertainty. Then the corresponding likelihood is

$$L(\sigma \times BR) = \iiint \prod_{i=bin} \prod_{j=bin} \frac{\mu_{ij}^{N_{ij}} \cdot e^{-\mu_{ij}}}{N_{ij}!} G(N_{QCD}, \sigma_{N_{QCD}}) G(N_{TOP}, \sigma_{N_{TOP}}) G(N_{Tc}, \sigma_{N_{Tc}}) dN_{QCD} dN_{TOP} dN_{Tc}, \quad (3)$$

We define the expected limit by taking the mean value of the iterated pseudo-experiment. We try to calculate expected limit with three b-tag condition (1 SECVTX tagging with NN tag, double tag, =1tag w/ NN tag & double tag combine). The limit of "=1tag w/ NN tag & double tag combine" are obtained by combining the two likelihood of L(σ|1tag) and L(σ|2tag) as

$$L(\sigma) = L(\sigma|1tag) \times L(\sigma|2tag)$$

where the correlation between 1 tag and 2 tag events are taken into account like in WH analysis. The systematic uncertainty up to the pretag acceptance, luminosity uncertainty and uncertainty of b-tag scale factor are considered to be 100% correlated between the two selection criteria. Figure 34 show the expected limit for three tag case. As WH analysis "=1tag w/ NN tag" combined with ">=2 tag" gives the best expected limit.

8.1 Observed limit

Finally, we set 95 % C.L upper limit on $\sigma(\rho_T^\pm \to W\pi_T^0) \times BR(\pi_T^0 \to b\bar{b})$ using combined likelihood 1tag w/ NNtag and double tag. In figure.35 the observed limit with combined

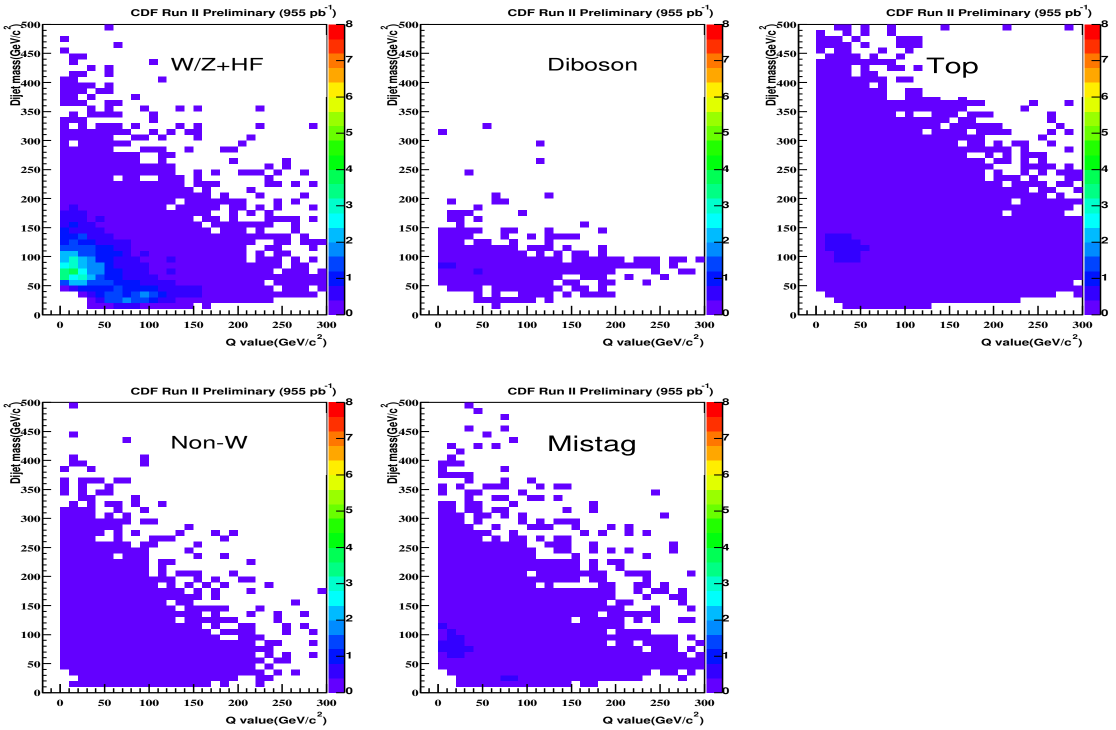

Figure 28: The reconstructed dijet mass vs. Q value ($m(\rho_T^{\pm})$-$m(\pi_T^0)$-m(W)) for each background components in exact 1 secVtx tag with NN tag.

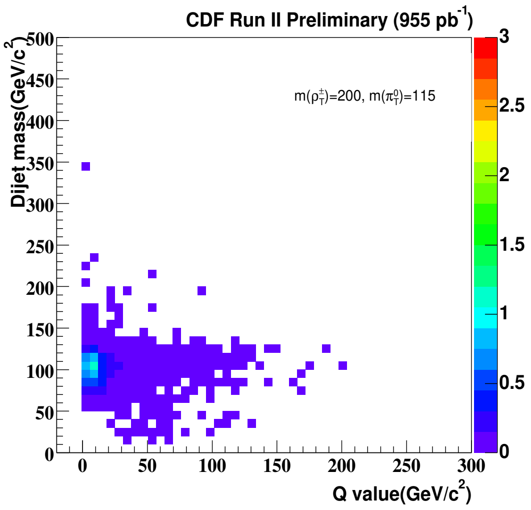

Figure 29: The reconstructed dijet mass vs. Q value ($m(\rho_T^{\pm})$-$m(\pi_T^0)$-m(W)) for signal nominal sample($m(\rho_T^{\pm})$=200,$m(\pi_T^0)$=115 GeV) in exact 1 secVtx tag with NN tag.

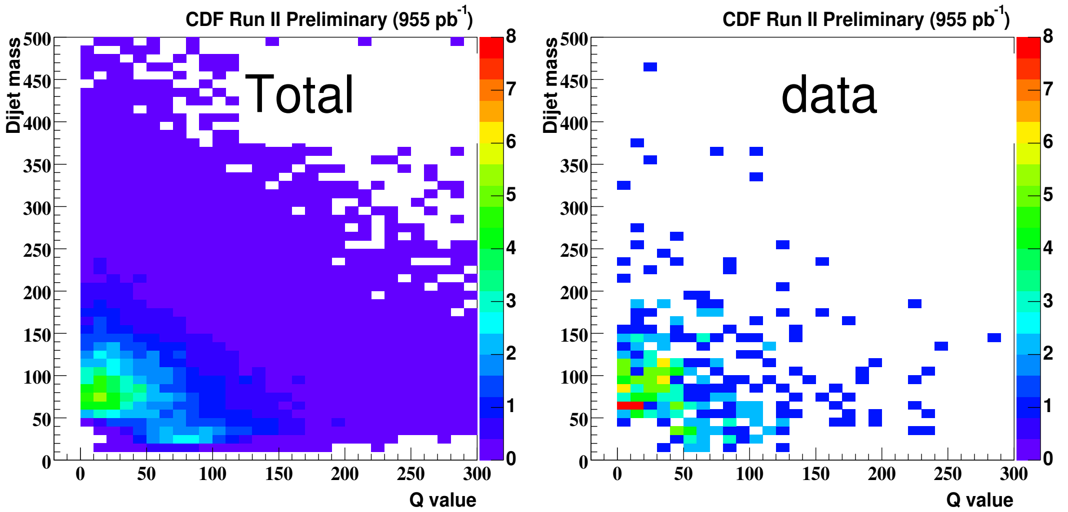

Figure 30: The reconstructed dijet mass vs. Q value ($m(\rho_T^{\pm})$-$m(\pi_T^0)$-m(W)) of total expected background in exact 1 secVtx tag with NN tag.

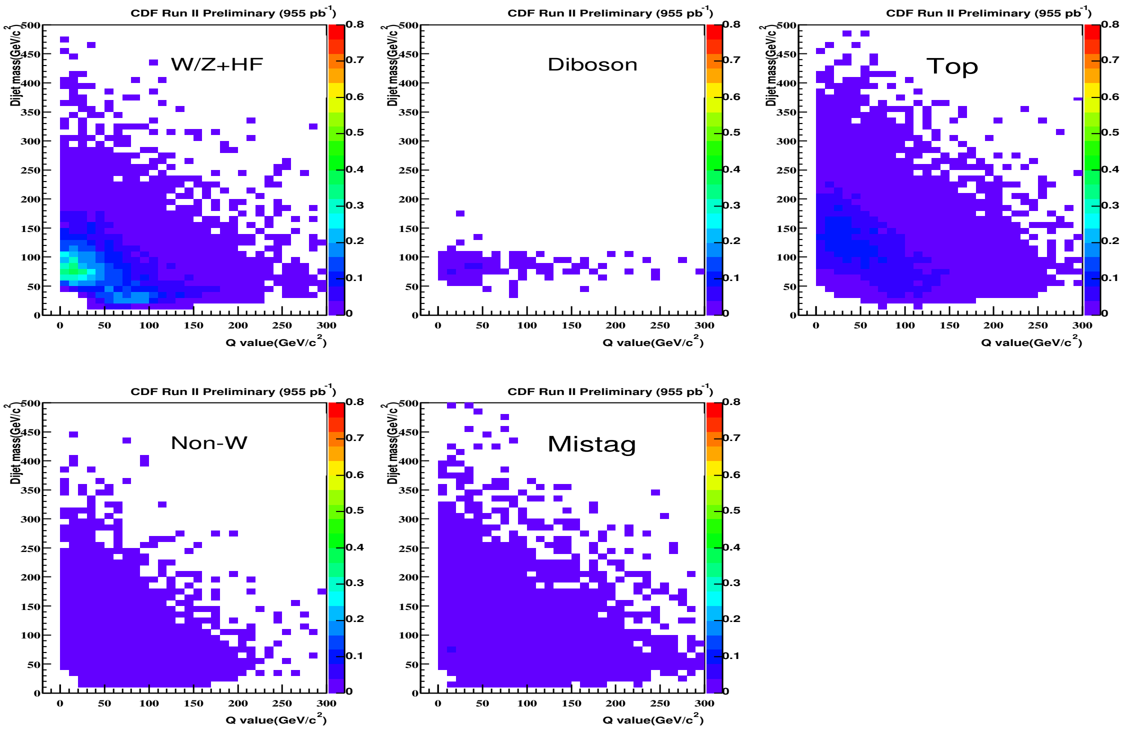

Figure 31: The reconstructed dijet mass vs. Q value ($m(\rho_T^{\pm})$-$m(\pi_T^0)$-m(W)) for each background components in double secVtx tag.

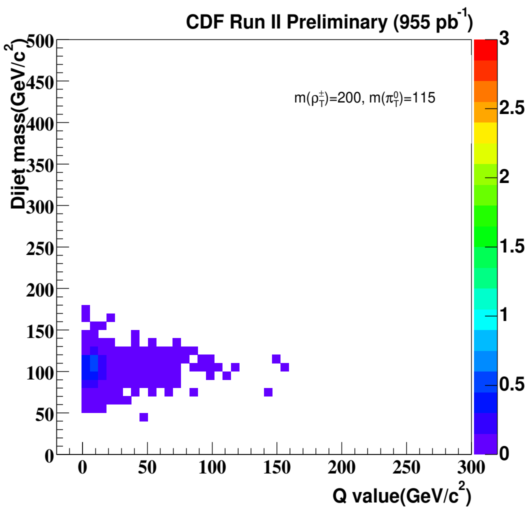

Figure 32: The reconstructed dijet mass vs. Q value ($m(\rho_T^\pm)$-$m(\pi_T^0)$-m(W)) for signal nominal sample($m(\rho_T^\pm)$=200,$m(\pi_T^0)$=115 GeV) in double tag.

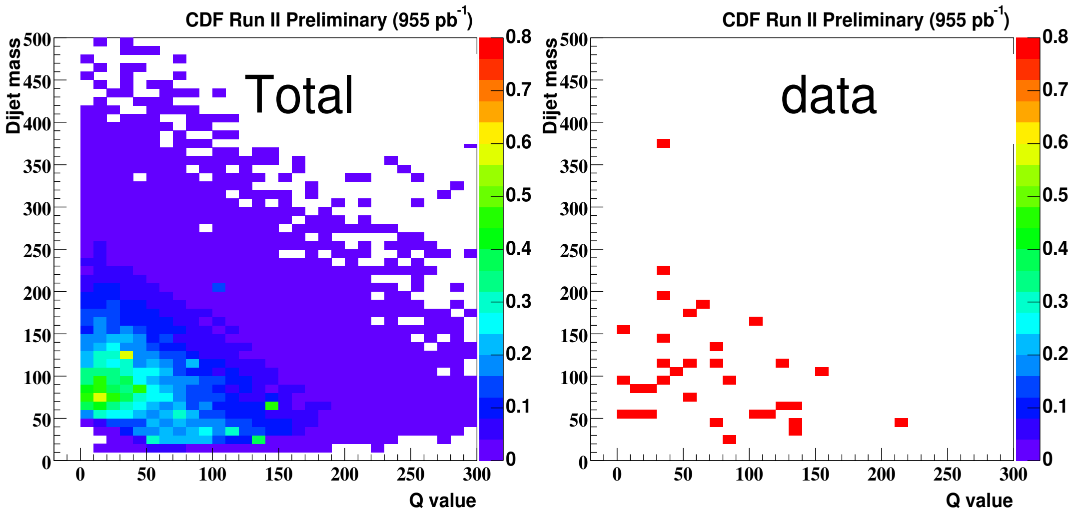

Figure 33: The reconstructed dijet mass vs. Q value ($m(\rho_T^\pm)$-$m(\pi_T^0)$-m(W)) of total expected background in double secVtx tag.

likelihood is shown as a function of $m(\pi_T^0)$ for each $m(\rho_T^\pm)$. To check if the obtained limit is reasonable or not, the result of pseudo experirment in same figure. Unfortunately, The observed limit we obtained is 2σ level highger than expected limit. Therefore we check the observed limit for 1tag w/ NNtag and double tag. In figure 37,38, the observed limit with 1tag w/ NNtag only and the results of pseudo experiments are shown. We can find the 2 σ higher observed limit in 1tag w/ NNtag. While the expected and observed limit with double

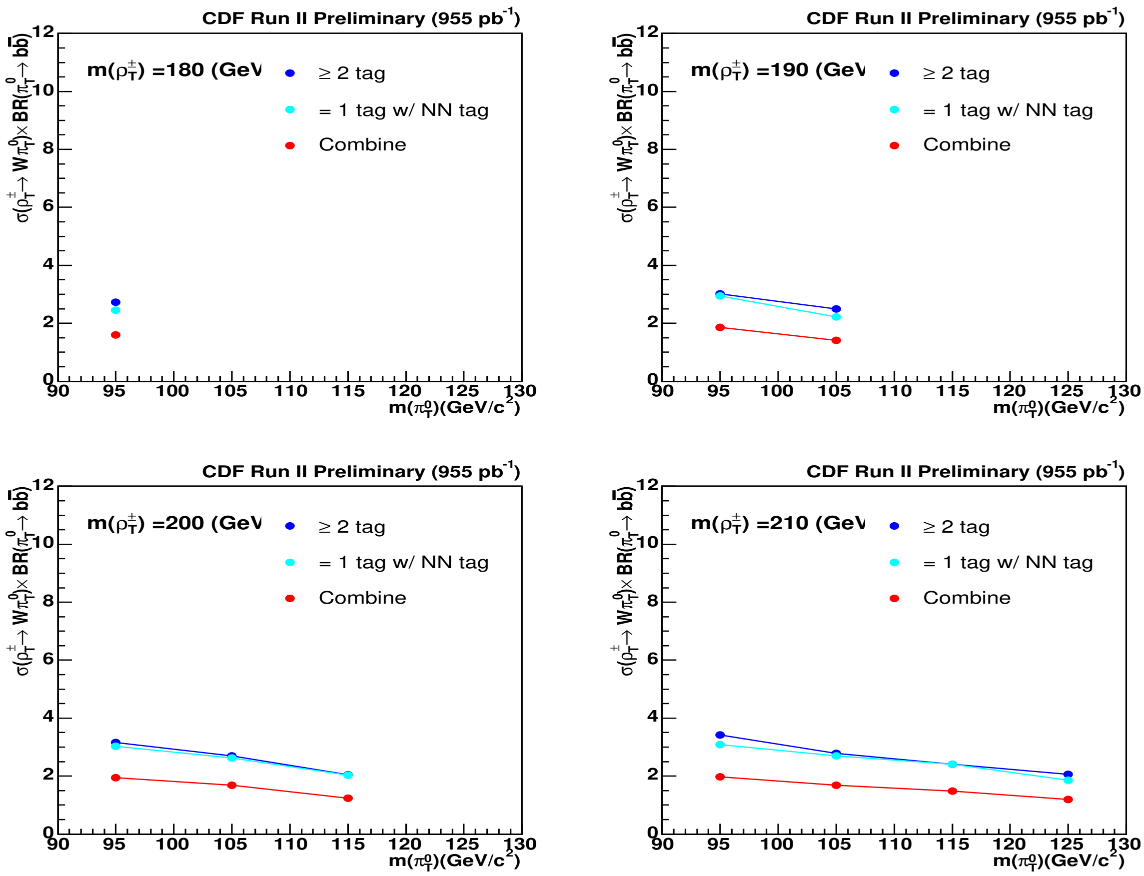

Figure 34: The expected limit as a function of Technipi mass $m(\pi_T^0\ )$ for 1 secVtx tag with NN tag, double secVtx tag and combined results for different Techni rho mass $m(\rho_T^\pm)$.

tag is shown in figure 39, 40, which seems reasonable.

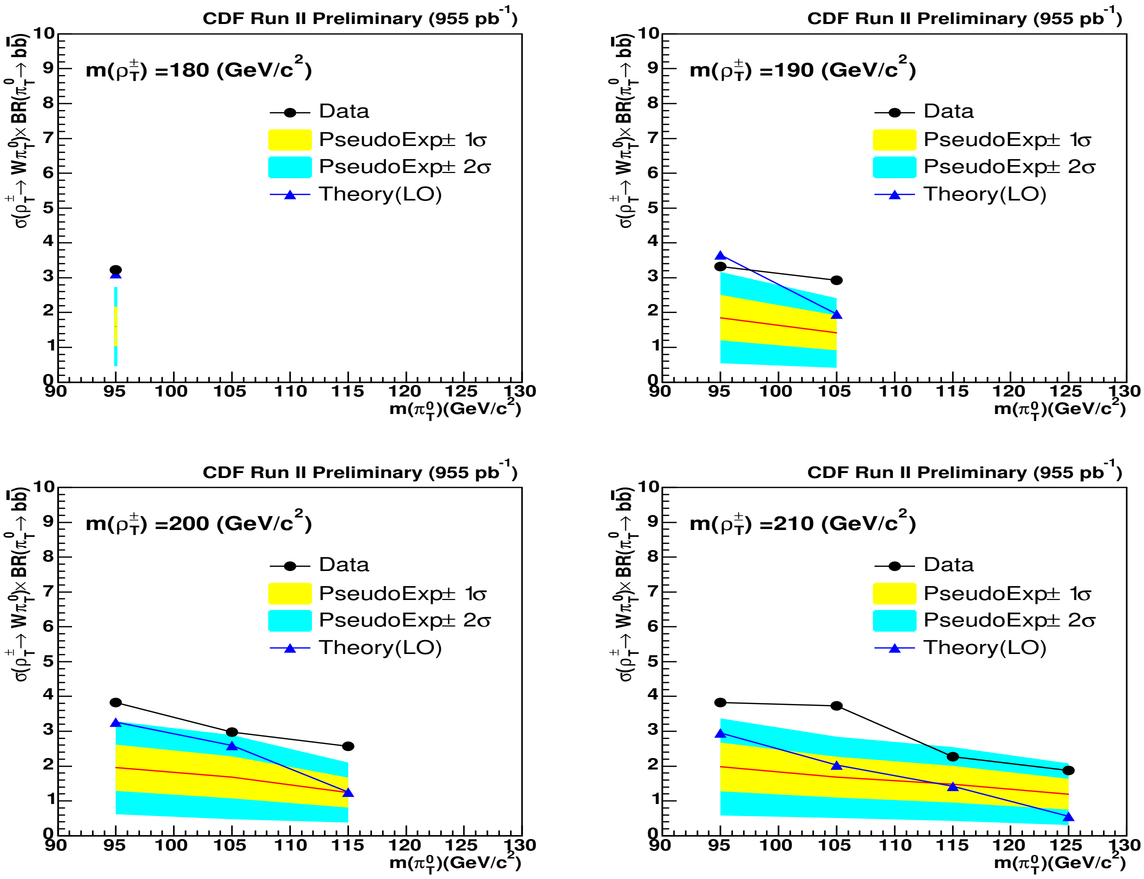

Figure 35: The expected and observed limit using likelihood combined 1 secVtx tag with NN tag and double secVtx tag, Theoretical cross section of leading order estimated from PYTHIA and observed limit calculated using 955 pb^{-1}

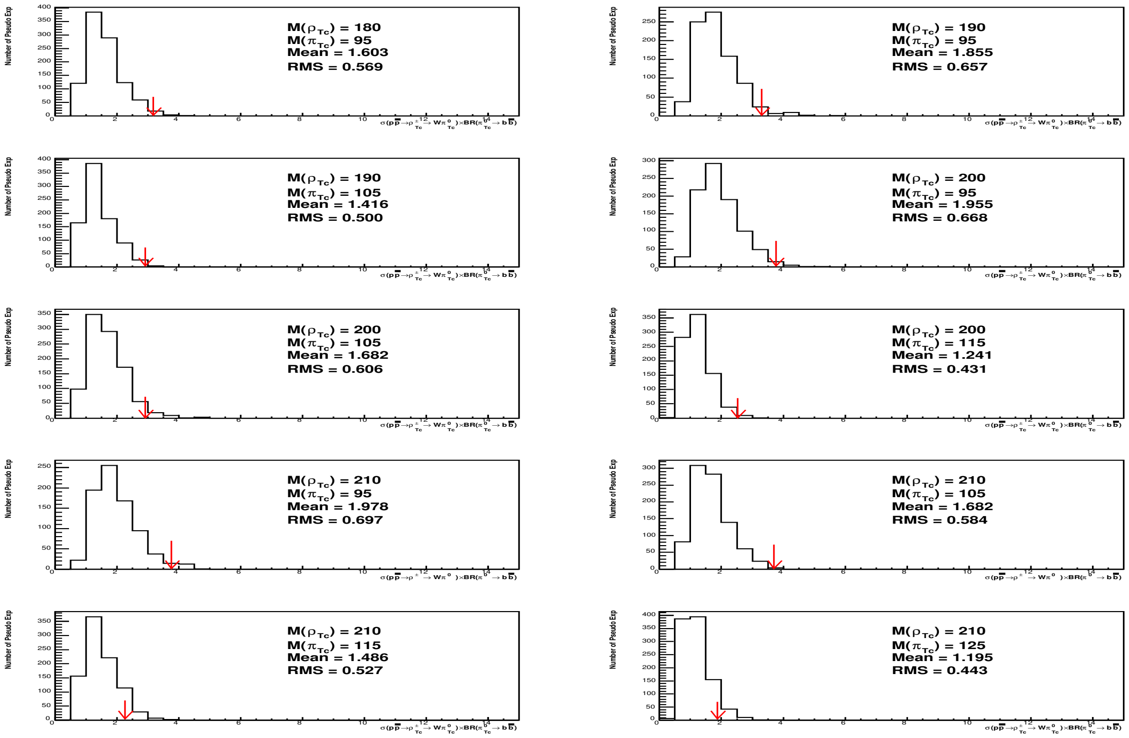

Figure 36: The results of one thousands pseudo experiments as a function of Technipi mass $m(\pi_T^0)$ for different Techinirho mass $m(\rho_T^\pm)$ using likelihood combined exact 1 secVtx tag with NN tag and double secVtx tag.

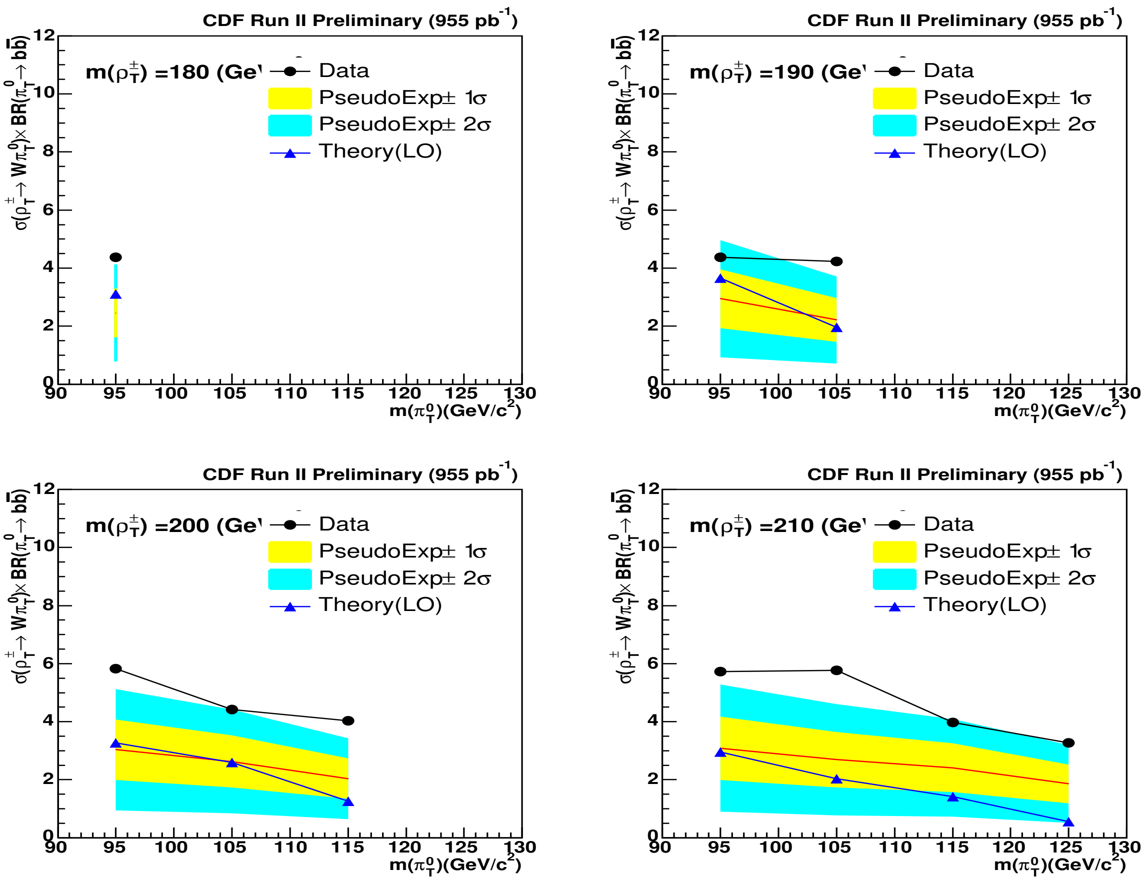

Figure 37: The expected and observed limit using likelihood with 1 secVtx tag with NN tag, Theoretical cross section of leading order estimated from PYTHIA and observed limit calculated using 955 pb^{-1}

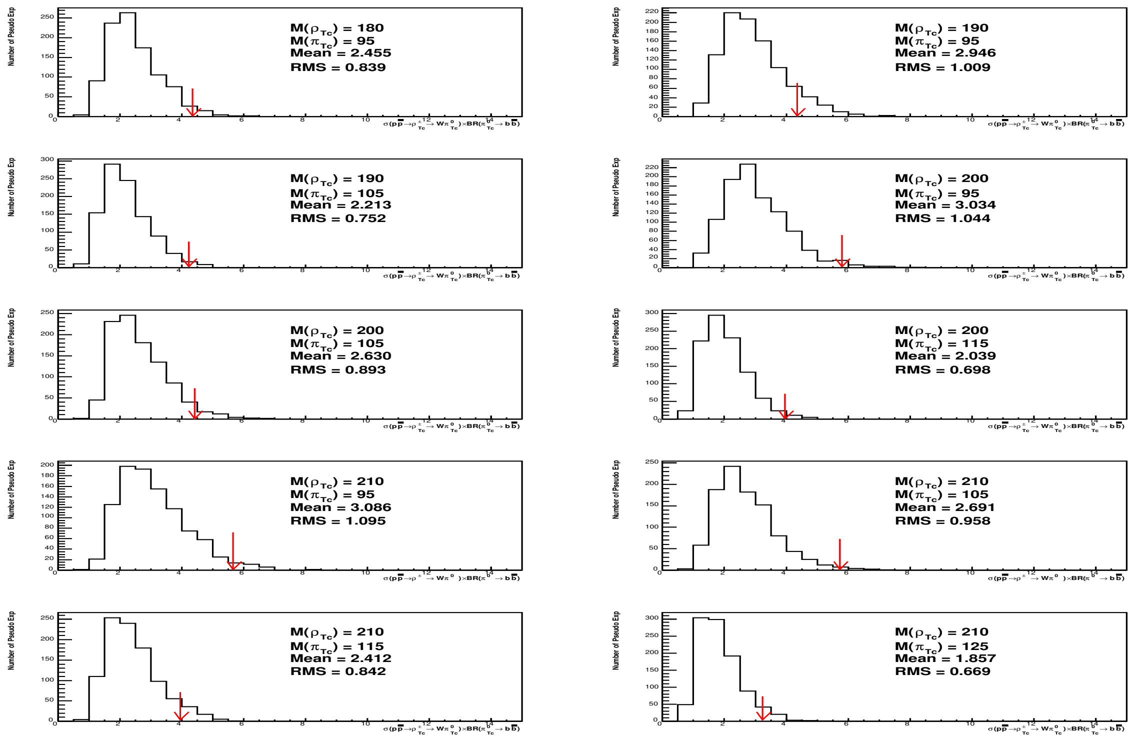

Figure 38: The results of one thousands pseudo experiments as a function of Technipi mass $m(\pi_T^0\ )$ for different Techinirho mass $m(\rho_T^\pm)$ in exact 1 secVtx tag with NN tag.

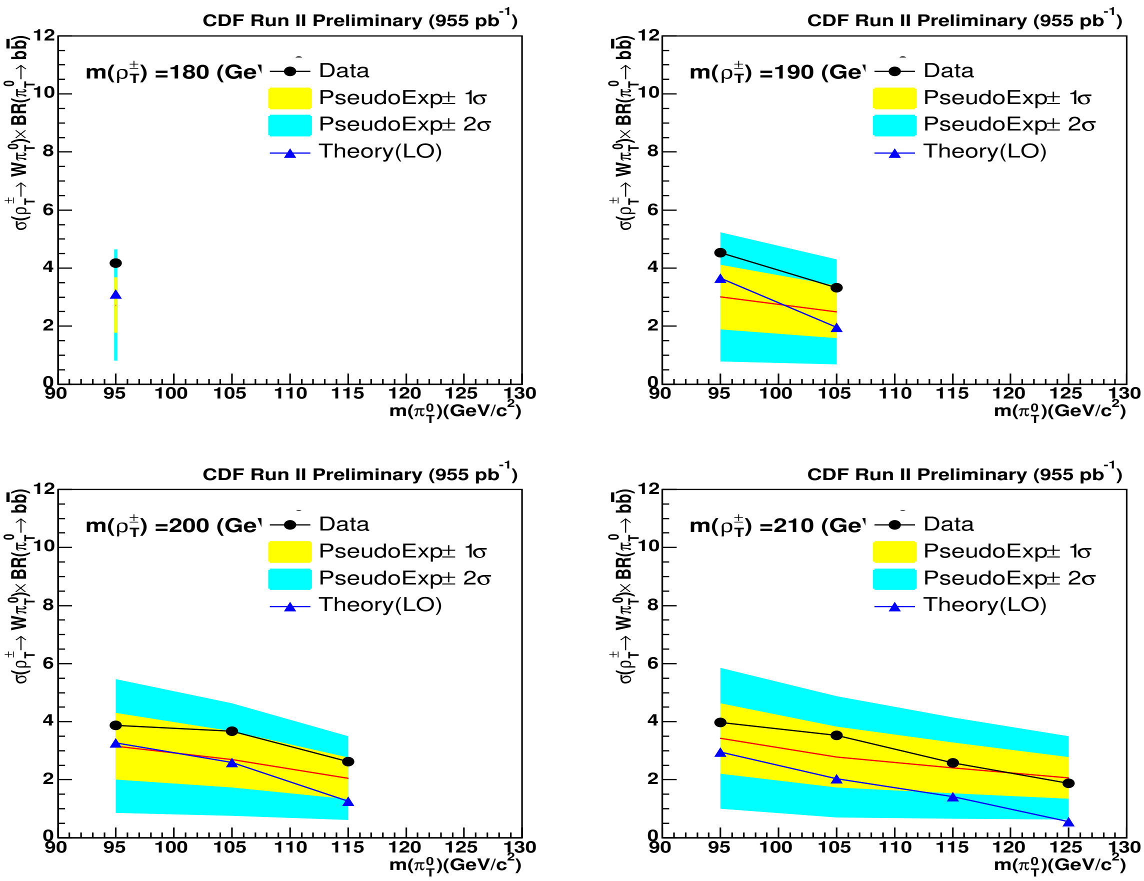

Figure 39: The expected and observed limit using likelihood with double secVtx tag, Theoretical cross section of leading order estimated from PYTHIA and observed limit calculated using 955 pb^{-1}

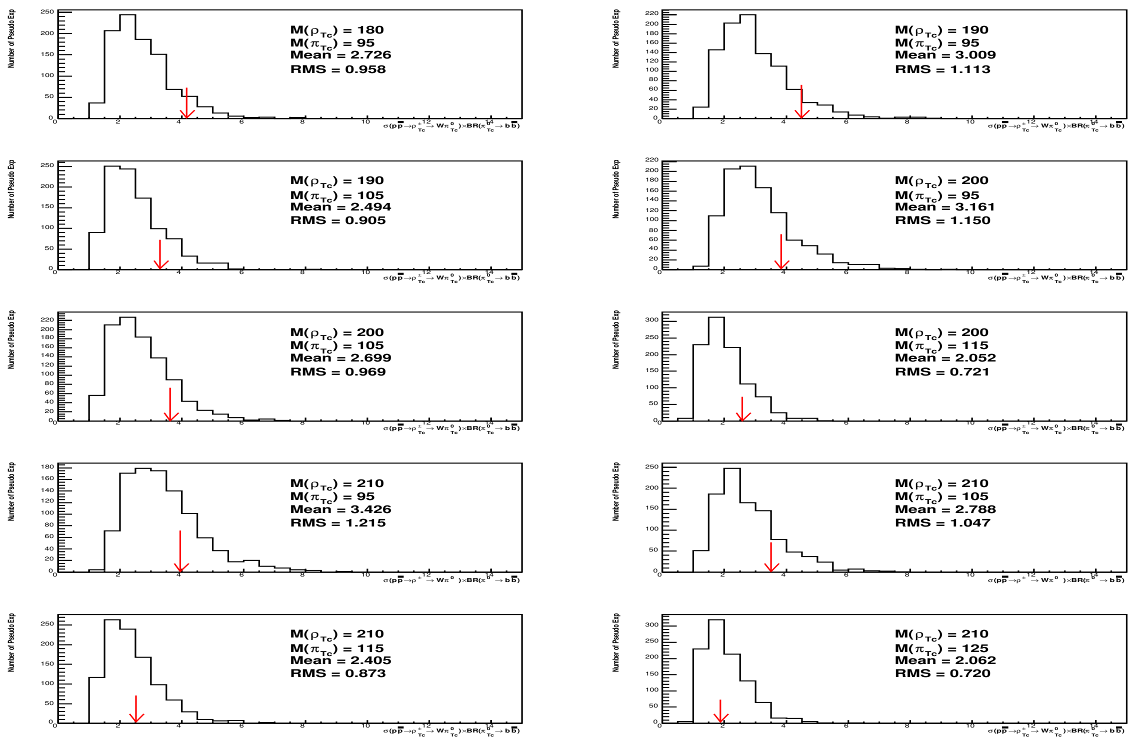

Figure 40: The results of one thousands pseudo experiments as a function of Technipi mass $m(\pi_T^0\ )$ for different Techinirho mass $m(\rho_T^{\pm})$ in double secVtx tag.

9 Cross check

9.1 Investigate the source of higher observed limit

Obviously the source of higher observed limit comes from 1tag w/ NN tag events, therefore we focus on 1tag w/ NN tag events and check some signal region to understagnd why observed limit is much higher than expected limit. Figure 41 shows dijet mass distributions after sliding Q value cut. There seems some excess of events near 100 GeV bins in dijet mass distribution. Figure 42 shows the same distribution with at least one tagged events. Other kinematics plots for at least one tags are shown in next section. We also checked the results dependent on the P_Z of neutrino by set it to zero. The results are almost identical to what we had in the default analysis. Figure 43,44 shows its Q value (Q') and dijet mass distributions after sliding Q' value cut.

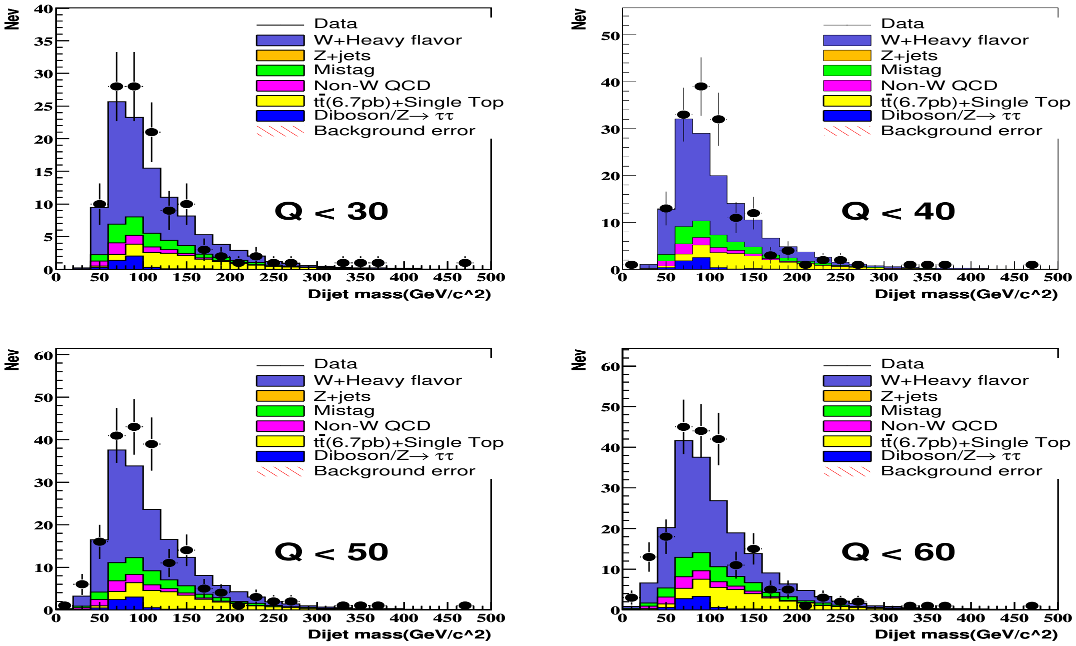

Figure 41: Dijet mass distrubutions after some Q cut on 1tag w/ NNtag

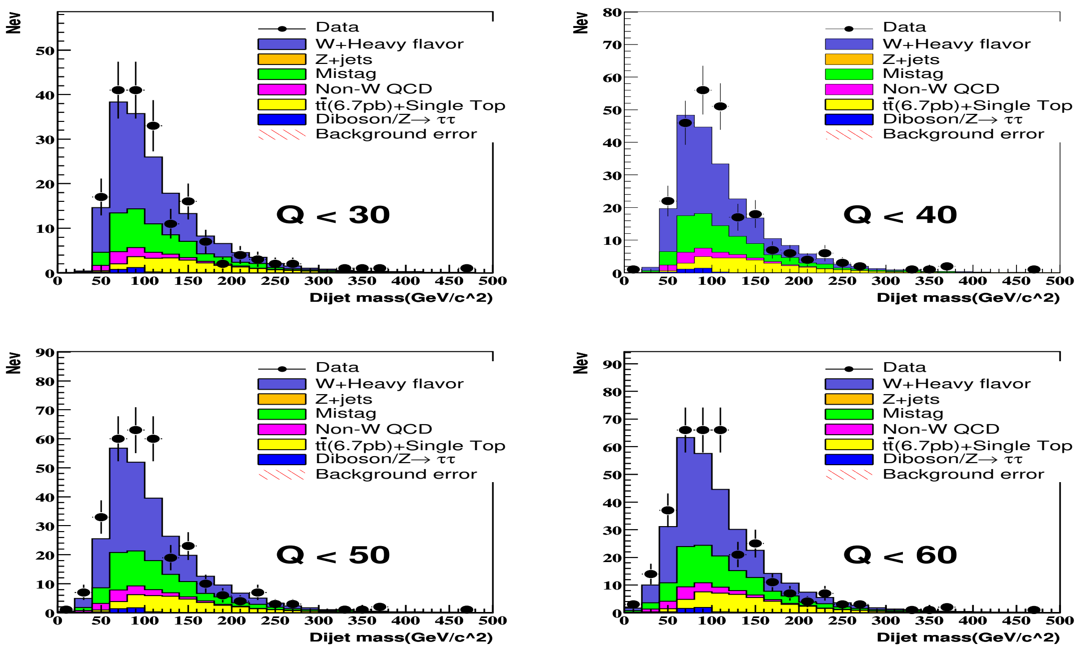

Figure 42: Dijet mass distrubutions after some Q cut on at least one tag

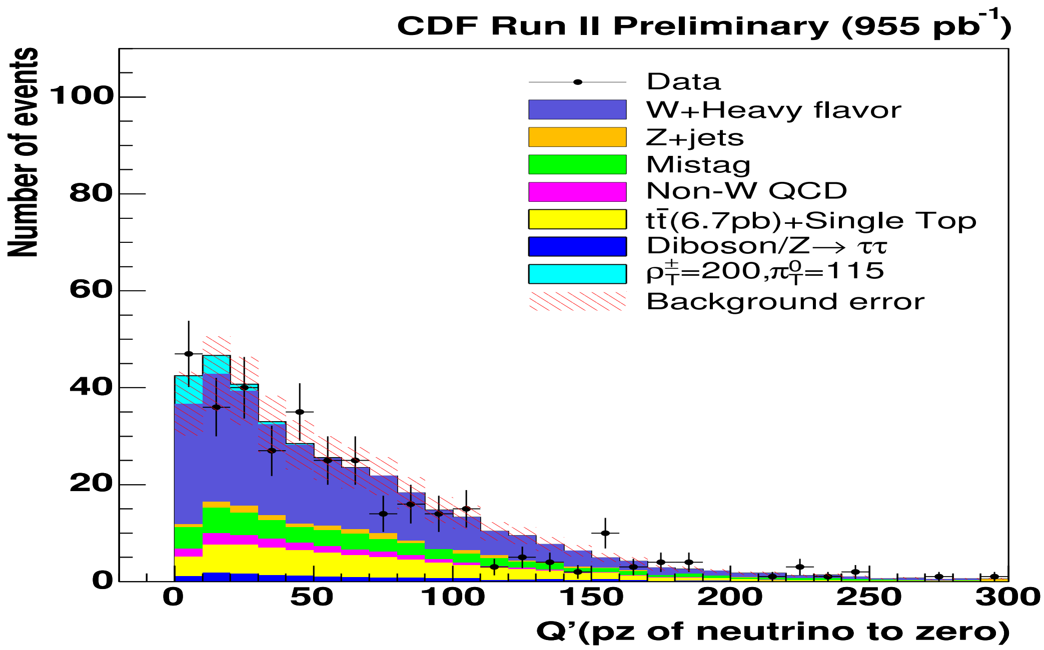

Figure 43: Q' value. Q' means the value calculated with the P_Z of neutrino bye set it to zero

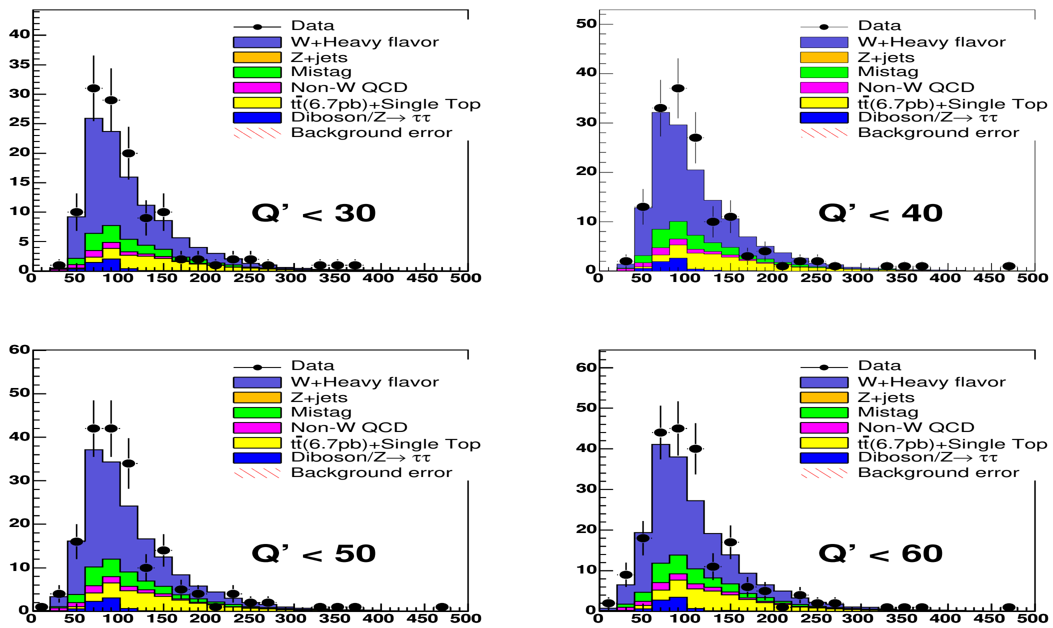

Figure 44: Dijet mass distrubutions after some Q' cut on 1tag w/ NNtag

9.2 At least one tag kinematic shape

We have checked the kinematic distributions with at least one SecVtx tagged events. The aim is to make sure the effect not caused by the neural network b-tagging. Overall the kinematics distributions we have looked so far are in good agreement between data and background expectations, which are shown in figure 45,46,50-57. In two dimentinal plot(figure 47-49) of Q value and dijet mass, the excess of events are consistent with the previous analysis with NN b-tagging.

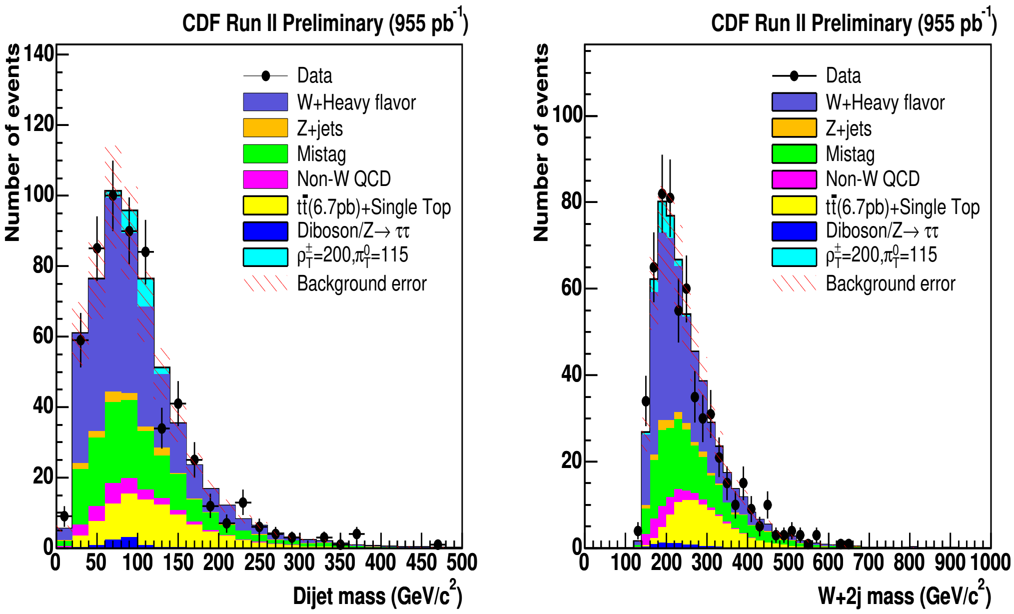

Figure 45: Dijet mass and W+2jet mass using 955pb^{-1} .

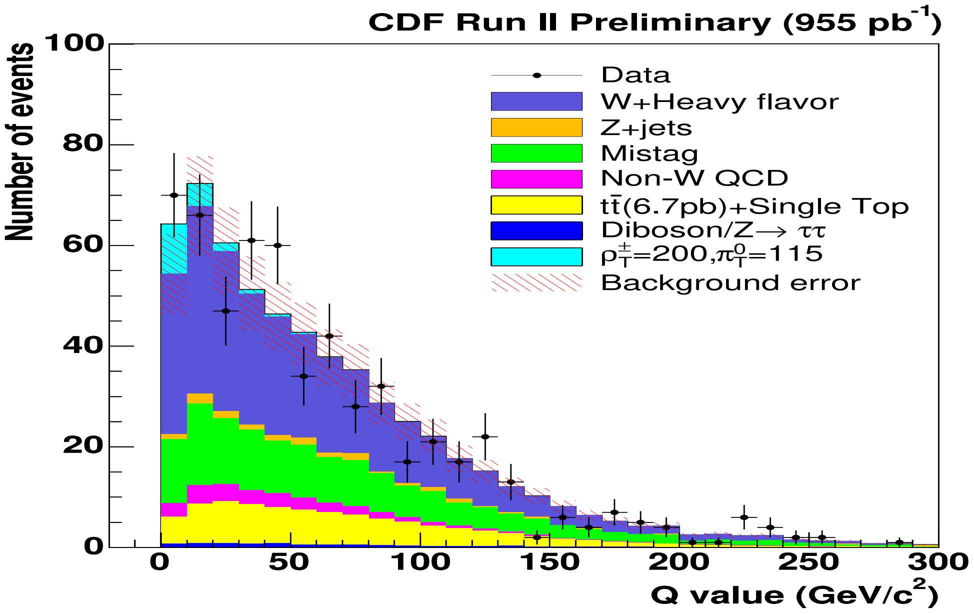

Figure 46: Q value using 955pb^{-1} .

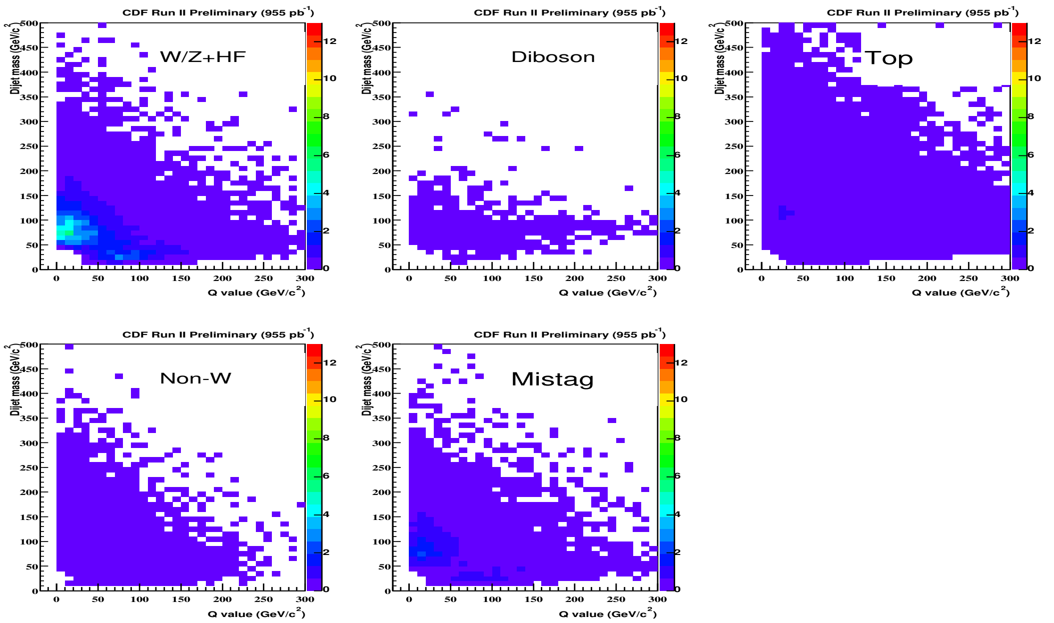

Figure 47: 2D plot of Qvalue and Dijet mass for each background components using 955pb^{-1}
.

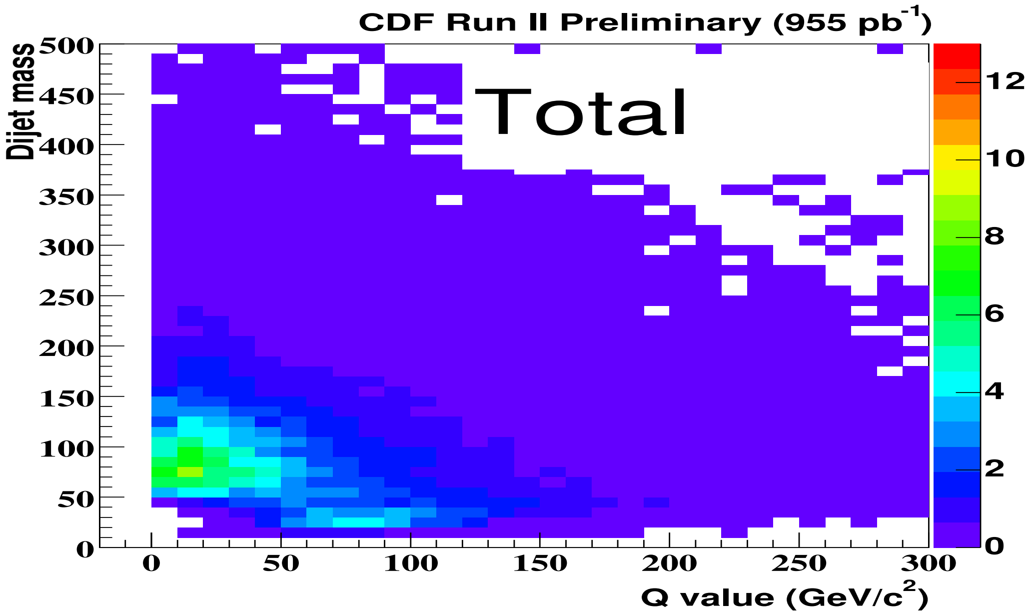

Figure 48: 2D plot of Qvalue and Dijet mass for total background using 955pb^{-1} .

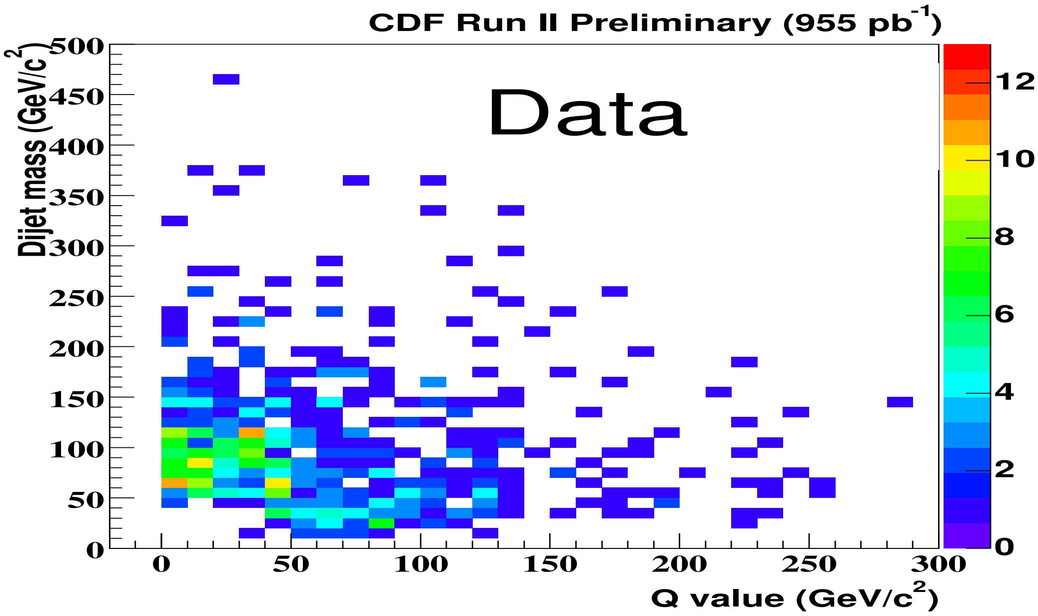

Figure 49: 2D plot of Qvalue and Dijet mass for observed data using 955pb^{-1} .

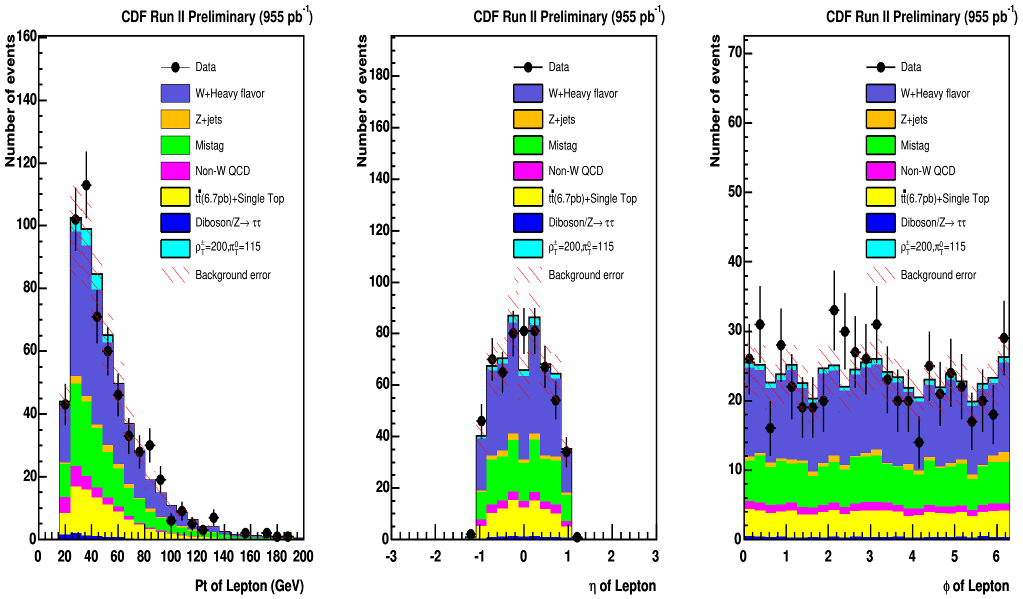

Figure 50: Lepton kinematics using 955pb-1 . From left Lepton p_T , η,ϕ. CEM, CMUP, CMX are included.

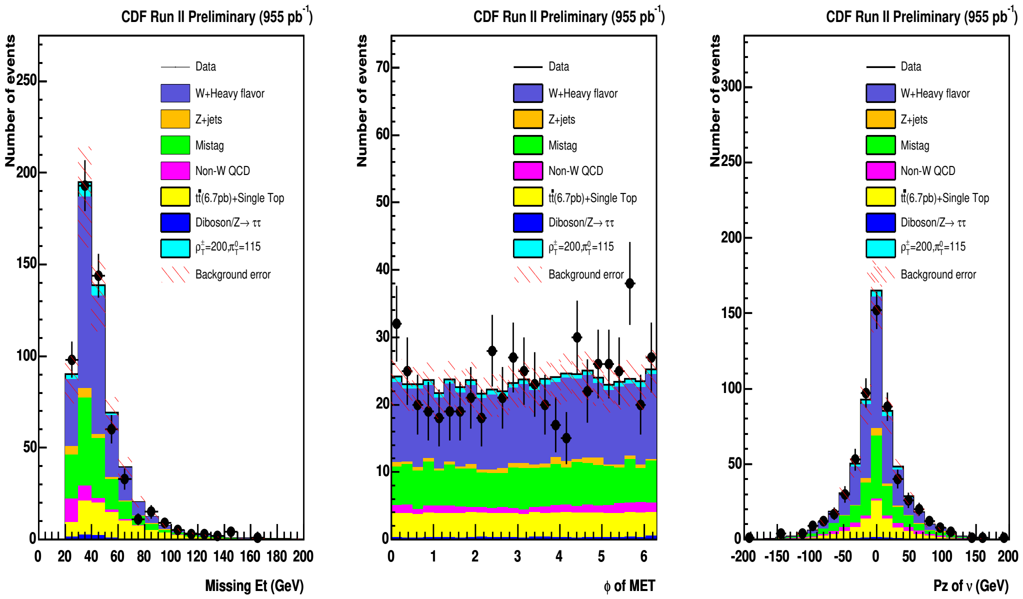

Figure 51: $\not\!\!E_T$ kinematics using 955pb-1 . From left, $\not\!\!E_T$, ϕ of $\not\!\!E_T$ and reconstructed pz of neutrino.

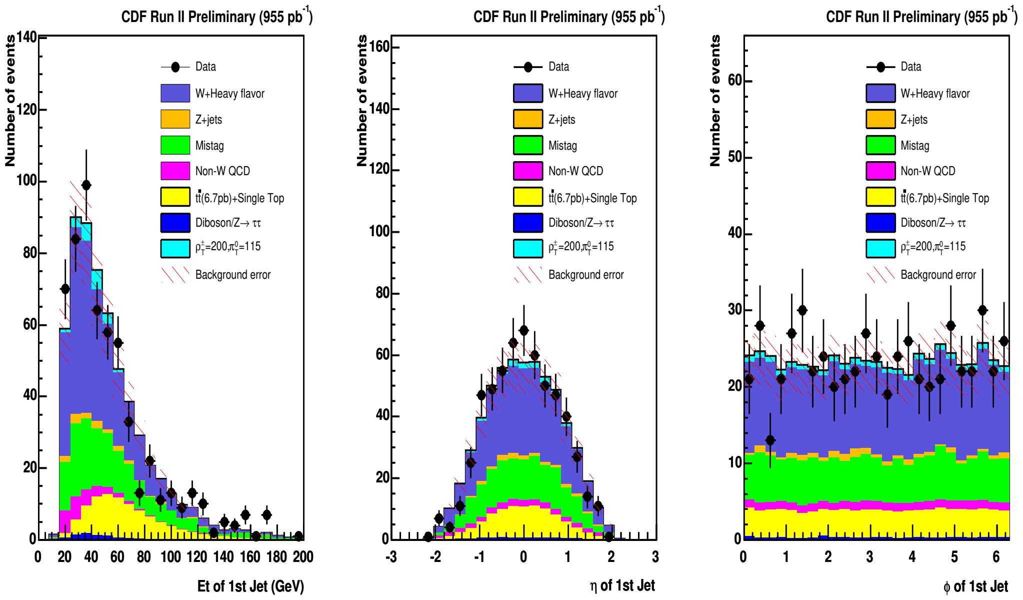

Figure 52: First leading jet kinematics using 955pb-1 . From left, E_T of jet, η of jet and ϕ of jet

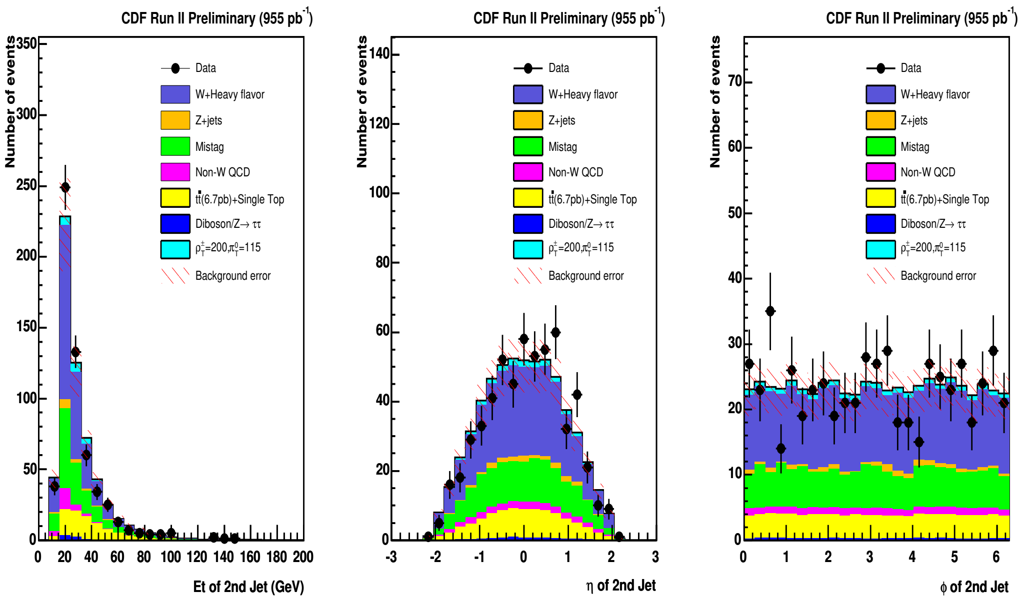

Figure 53: Second leading jet kinematics using 955pb-1 . From left, E_T of jet, η of jet and ϕ of jet

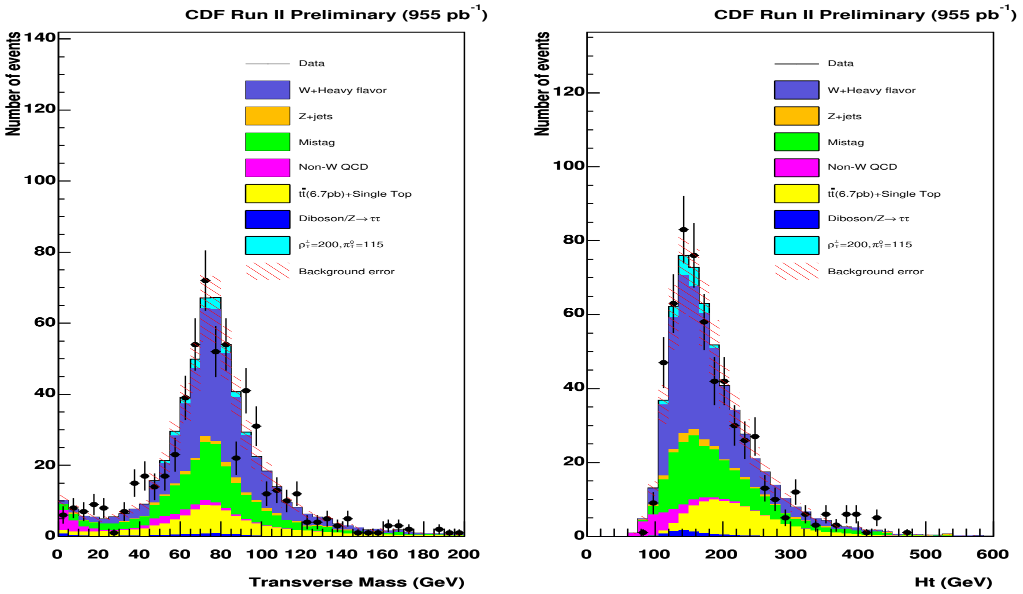

Figure 54: Transverse mass and Ht using 955pb^{-1}

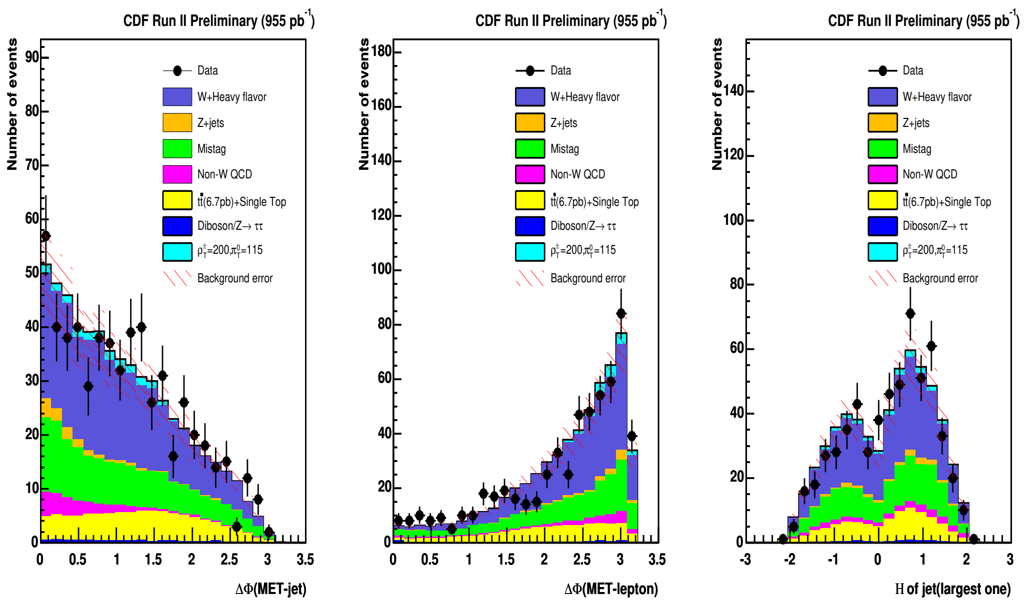

Figure 55: From left, $\Delta\phi$ between $\not{E}_T$ and closest jet, $\Delta\phi$ between $\not{E}_T$ and lepton and η of jet with largest η using 955pb^{-1}

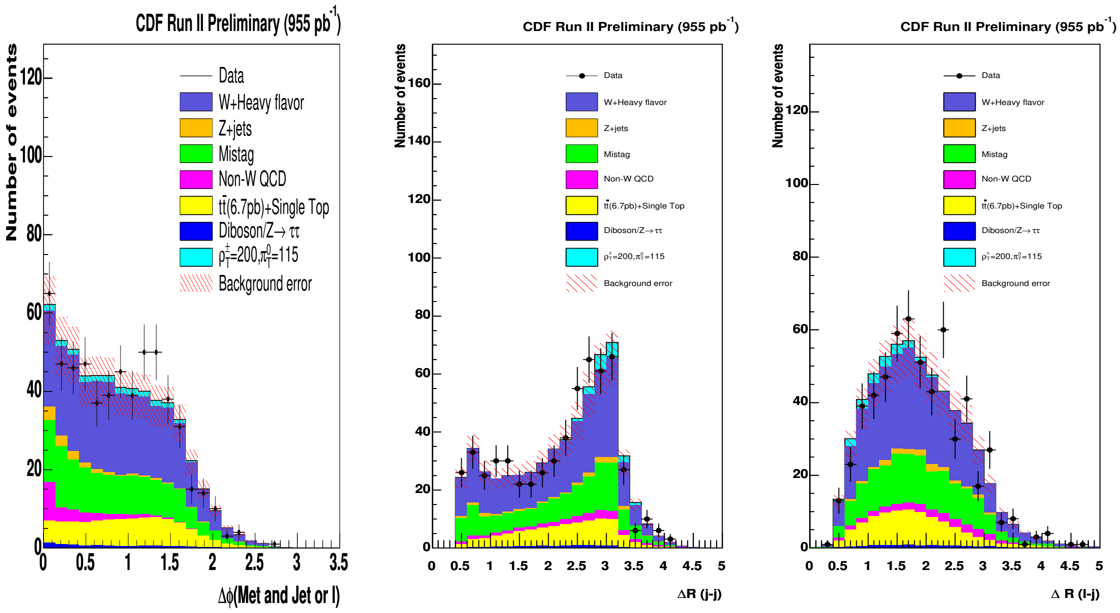

Figure 56: Minimum $\Delta\phi$ between $\not{E}_T$ and lepton or jets, ΔR between 1st jet and 2nd jet, ΔR between lepton and closest jet using 955pb-1

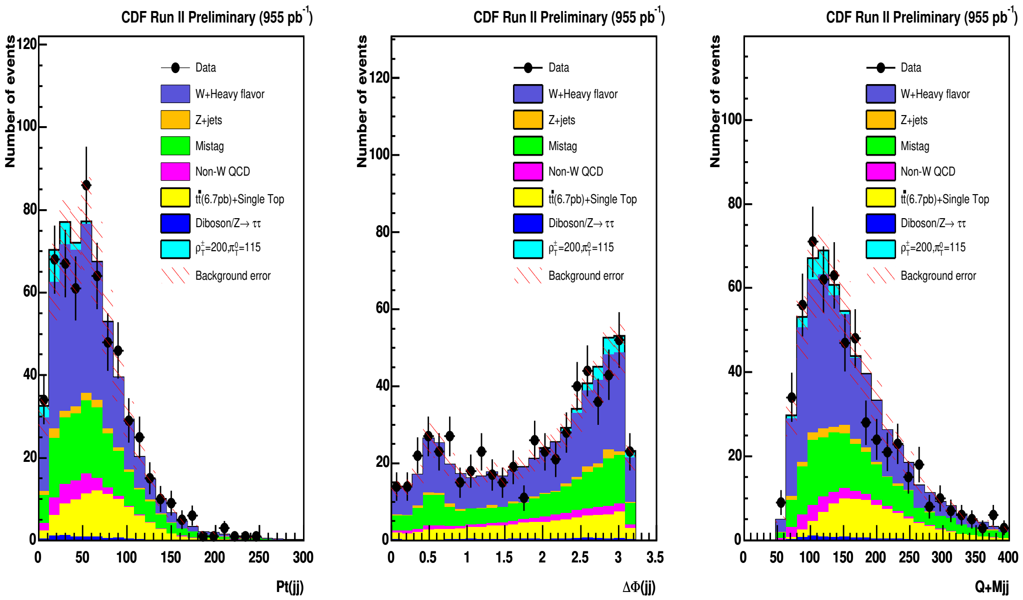

Figure 57: $\Delta\phi$ between 1st jet and second jet, p_T of dijet using 955pb-1

9.3 How significant is the excess from the data (p-value) ?

Since there is no prior knowledge of technicolor particle masses we need to check how significant the obseved limit we got in whole $m(\rho)$,m(π) plane using pseudo-experiments. For each pseudo experiment, we estimate the observed 95% CL limit ,compute the p-value against the prior distribution and record the smallest p-value for all the possible masses. Figure 58 shows the p-value in log scale for all the psuedo experiment. We found 2.6% of pseudo-experiments having the p-value equal or less than what observed in data (0.3%).

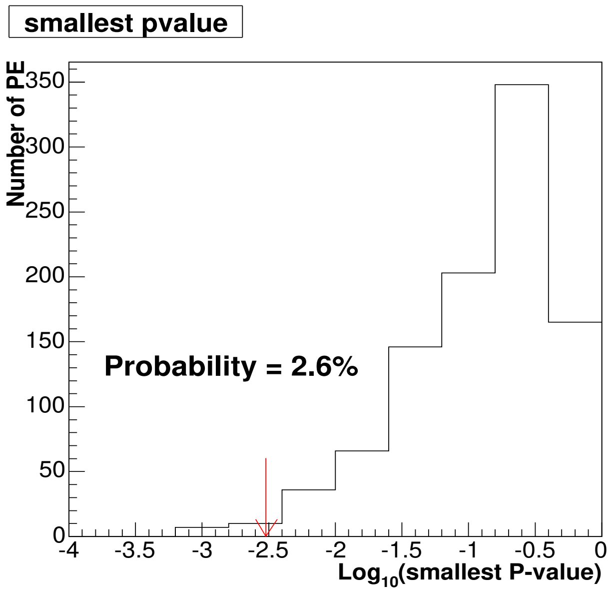

Figure 58: Smallest p-value into all mass sample for pseudo experiment. Red arrow means smallest observed p-value on combined limit

10 Conclusions

We have presented a search for the Technicolor particles (Techni rho and Techni pion) using $\approx 1fb^{-1}$ data. We find that the observed events agree with our background predictions. We set an upper limit on the production cross section times branching ratio as function of techinicolor particle masses. We are able to exclude some Technicolor mass region with 95% C.L. The excluded region is listed in table6. The observed limit is much worse than the expected due to some excess of events in some mass region, but the statistical significance of such excess is about 2.6%.

$m(\rho_T^{\pm})$	$m(\pi_T^0)$ exclude region at 95% C.L.
190 GeV	$95 < m(\pi_T^0) < 98$ GeV

Table 6: The excluded region at 95% C.L in the ($m(\rho_T^{\pm})$-$m(\pi_T^0)$) plane for $\rho_T^{\pm} \to W\pi_T^0 \to l\nu b\bar{b}$ production

References

[1] Kenneth Lane, "Search for Low-Scale Technicolor at the Tevatron", hep-ph/0605119

[2] Y. Ishizawa, W. Yao., "Search for Technicolor Particle in $W^{\pm} + 2$ Jets with Secondary Vertex b-tagging", CDF Note 7092

[3] Y. Kusakabe it et al., "Search for Standard Model Higgs Boson Production in Association with W$^{\pm}$ Boson at CDF with $\int \mathcal{L}dt$ = 695 pb^{-1}, CDF Note 8194

[4] Y. Kusakabe it et al., "Search for Standard Model Higgs Boson Production in Association with a W$^{\pm}$ Boson at CDF with $\int \mathcal{L}dt$ = 1.0 fb^{-1}, CDF Note 8355

[5] H. Bachacou, P.Lujan, M.McFarlane, W.Yao, "Advanced Heavy Flavor Tagging Using a Neutral Network", CDF Note 7742

[6] M. McFarlane et al. "Measurement of ttbar cross section with NN btagging in Lepton + jets events", CDF Note 8188

[7] V. Boisvert, "Trigger Efficiencies for the High E_T Central Electron in Gen6", Cdf Note 7939

[8] J.Incandeta C.Hill and C.Mills "Electron identification in offline release 5.3.1" CDF note 7031

[9] U. Grundler, A. Taffard, and X. Zhang, "High-Pt muons recommended cuts and efficiencies for winter 2006" CDF note 7956

[10] C. Neu et al., "Combination of the SECVTX b-Tagging Scale Factors for Wimter 2006 Analysis", CDF note 8025

[11] H. Bachacou, C. Feretti, J. Nielse, W.Yao, "Heavy Flavor contributions to the SECVTX-tagged W+Jets sample" CDF note 7007

[12] D. Acosta et al. "First Measurements of Inclusive W and Z Cross section from RunII of Tevatron Cllider", hep-ex/0406078

[13] Sara Budd et al. "Estimation and modeling of non-W background for single top searched", CDF note 8489

[14] Peter Dong, Bernd Stelzer "Reduction of QCD background in lepton + jets events", CDF note 8295

[15] Sara Budd et al. "Data Based background estimate for Summer 2006 Single-Top Search"